COMPENSATION OF MUTUAL COUPLING IN TRANSMITTING ARRAYS OF THIN WIRE ANTENNAS

A THESIS SUBMITTED TO

THE GRADUATE SCHOOL OF

ENGINEERING AND NATURAL SCIENCES

OF ISTANBUL MEDIPOL UNIVERSITY

IN PARTIAL FULFILLMENT OF THE REQUIREMENTS FOR

THE DEGREE OF

MASTER OF SCIENCE

IN

ELECTRICAL, ELECTRONICS ENGINEERING AND CYBER SYSTEMS

By

Sana Khan

August, 2017

ABSTRACT

COMPENSATION OF MUTUAL COUPLING IN TRANSMITTING ARRAYS OF THIN WIRE ANTENNAS

Sana Khan

M.S. in Electrical, Electronics Engineering and Cyber Systems

Advisor: Prof. Dr. Ercümend Arvas

August, 2017

In the classical approach of antenna array theory, mutual coupling between elements is usually ignored. However, depending on the application, errors due to mutual coupling can be significant. This thesis presents a numerical study for the compensation of mutual coupling between elements in small dipole arrays using Method of Moment. By using the mutual impedance of the antenna elements, it is possible to compute a new set of excitation voltages. Using these new *compensated voltages* one can obtain the pattern that would be similar to the pattern obtained by the original voltages if there were no mutual coupling. This compensated pattern is compared with the radiation pattern obtained using pattern multiplication method which does not include mutual coupling. In this thesis, mutual coupling has been compensated for different array configurations including linear arrays, circular arrays as well as 3-Dimensional arrays. Individual element of the arrays can have different length, radius and relative positions in space.

ÖZET

VERİCİ İNCE TEL ANTEN DİZİLERİNDE KARŞILIKLI BAĞLANMANIN TAZMİN EDİLMESİ

Sana Khan

Elektrik Elektronik Mühendisliği ve Siber Sistemler, Yüksek Lisans

Tez Danışmanı: Prof. Dr. Ercümend Arvas

Ağustos, 2017

Anten dizisi teorisinin klasik yaklaşımında, öğeler arasındaki karşılıklı bağlanma genellikle dikkate alınmaz. Bununla birlikte, uygulamaya bağlı olarak, karşılıklı bağlantıdan kaynaklanan hatalar önemli olabilir. Bu tez, Moment Metodu'nu kullanarak küçük dipol dizilerindeki elemanlar arasındaki karşılıklı bağın tazmini için sayısal bir çalışma sunmaktadır. Anten elemanlarının karşılıklı empedansını kullanarak yeni bir uyartım gerilimi seti hesaplamak mümkündür. Bu yeni dengelenmiş gerilimleri kullanarak, karşılıklı bir bağlanma olmasaydı orijinal gerilimlerle elde edilen desene benzer bir model elde edebilir. Bu dengelenmiş desen, karşılıklı eşleşme içermeyen çarpma metodu deseni kullanılarak elde edilen radyasyon deseni ile karşılaştırılır. Bu dengelenmiş desen, karşılıklı eşleşme içermeyen çarpma metodu deseni kullanılarak elde edilen radyasyon deseni ile karşılaştırılır. Bu tezde, karşılıklı bağlantı, doğrusal diziler, dairesel diziler ve 3 Boyutlu diziler de dahil olmak üzere farklı dizi yapılandırmaları için telafi edilmiştir. Dizilerin bireysel elemanları, uzaydaki farklı uzunluk, yarıçap ve göreli konumlara sahip olabilir.

Acknowledgement

I am grateful to my advisor Prof. Dr. Ercümend Arvas for his relentless efforts in guiding me and enabling me to take up this endeavor. Despite my shortcomings he never gave up on me. Thank you Sir.

I am thankful to my parents for letting me earn my dreams...My family and friends who always instilled hope in me in gloomy days. Last but not the least, I am thankful to my husband who has stood besides me through this whole journey.

To my father, who taught me to never give up. . .

Contents

List of Figures

List of Tables

Chapter 1

Introduction

Antenna arrays have a wide range of applications involving commercial and military applications [1],[3]. They are used in systems such as radio, television broadcasting, weather research, radar, missile guidance systems and space communications. Due to miniaturization of electronic devices, small-sized antenna arrays also called as compact antenna arrays has attracted a lot of interest. One such example of compact antenna arrays is called Multiple Input Multiple Output (MIMO) system. In conventional wireless communications, a single main antenna was used to transmit and receive data. Nowadays, mobile phones or smart phones provide us with multiple services. These services include GPS, WiFi, Bluetooth, Infrared etc. All of these services require an antenna in order to receive and transmit data. In the current industry, the single main antenna has been evolved to multiantenna solution as MIMO. In a MIMO system these multiple antennas are placed at a close proximity inside the handset. Due to the small distance between the antenna elements they interact with one another. This electromagnetic interaction is called mutual coupling. This interaction changes the current magnitude, phase, and distribution on each element from their free space values. As a consequence, total array pattern is altered. Compact antenna arrays suffer from mutual coupling which can alter the overall radiation pattern, gain, bandwidth and impedance matching of the antenna. Mutual coupling between the antenna elements in an antenna array is a classic problem which is responsible for the degradation of array performance [4], [5], [6]. In the classical array theory, it is often taken that the radiation pattern of an array of identical antenna elements is the product of an element pattern and an array factor. The element pattern is the pattern of an isolated element with center usually at origin. This element is assumed to be excited by a unit voltage. The array factor is a sum of fields from

isotropic point sources located at center of each array element and is found from the element voltages (amplitudes and phases) and their locations [1]. Therefore, in the classical array theory, it is assumed that all the elements of the array have equal radiation pattern, in other words, the coupling between individual elements is ignored. For a practical array, this is not entirely true since mutual coupling causes each element to see a different environment and consequently has a different radiation pattern from its neighboring elements. Several techniques to reduce mutual coupling and improve the isolation have been investigated [7], [8]. Some of them are given below:

- **Decoupling Networks (DN):** These networks use lumped elements and hybrid couplers to reduce mutual coupling. It has a disadvantage of narrow bandwidth. Parallel resonant circuits can be used to achieve broad bandwidth. Strips and slots introduce different resonances at different frequencies to help increase the isolation.

- **Defected Ground Plane Structure (DGS):** In this technique ground plane is modified by introducing slits of different shapes. This modification creates a band-stop filter and suppresses the coupling fields.

- **Parasitic Elements**: Inductance and capacitance is introduced using Electromagnetic Band Gap (EBG) to create a forbidden band of frequencies which helps in isolation of the antennas.

- **Meta-materials**: These are materials with special properties, e.g., negative permittivity or permeability or both. They are used due to existence of band gaps in their frequency response. The band gaps act as band notch filters and destroy mutual coupling between the elements. Mostly used structures are split ring resonators (SRR) and complementary split ring resonators (CSRR). Due to the substrate there is a deterioration of bandwidth.

- **Neutralization Lines (NL)**: In this technique current at the input element is taken at a location where impedance is minimum and current is maximum and then its phase is reversed by choosing suitable length of NL. The reversed current is then fed to nearby antenna to lessen the amount of coupled current. This method has a narrow bandwidth and the location of maximum current is difficult to find.

All the techniques mentioned above increase complexity of the network one way or the other. Physical modification of the structure is required by introducing lumped elements, parasitic

elements or special materials may be needed to reduce the coupling. This dissertation uses a non-invasive method in which the physical structure or design of the antenna is not changed. Neither any special materials or elements are required. Instead, only the excitation voltages of the antenna are changed and these new excitation voltages which are called compensated voltages produce a radiation pattern which is very similar to the pattern obtained from pattern multiplication method. In summary, the array factor method gives us the theoretical pattern of antenna arrays without mutual coupling. The real practical pattern is different from the theoretical pattern because of mutual coupling. In order to make the real practical pattern similar to our desired theoretical pattern, we compensate for the mutual coupling.

This thesis considers arrays of thin wire dipole antennas with length less than or equal to $\lambda/2$. Such antennas are usually called as single mode antennas. The individual elements in the array may not be identical in length, radius or position. A number of methods have been suggested for the compensation of mutual coupling [6], [9] and [10]. Here a numerical method has been used to compensate for mutual coupling, called Method of Moments (MoM). By using thin wire approximation the exact integral equation is solved approximately using MoM which helps us to compute the current distribution on the thin wire antennas. This gives us the radiation pattern in the presence of mutual coupling. Using the moment matrix for the array, we can calculate the coupling effect in terms of scattering matrix which is then used to find the new input voltages or compensated voltages to the antennas. When the antennas are excited by these new voltages it is observed that the pattern is similar to the theoretical pattern which we expect using the array factor theory and thus compensation is achieved.

1.1 Motivation
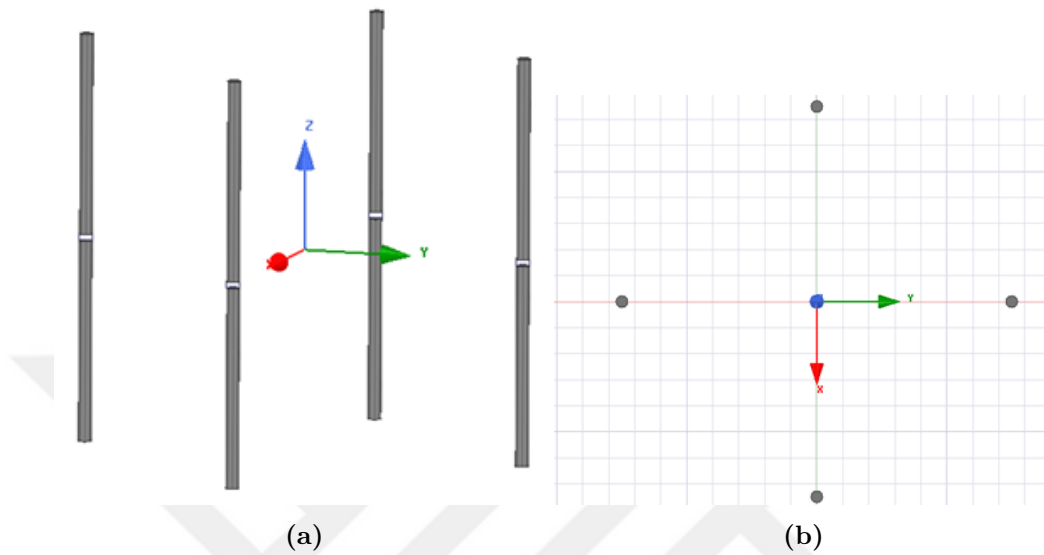
Figure 1.1: Circular array of four half-wave dipoles with radius of circle $\lambda/4$. a) Side View. b) Top View.

Figure 1.1 shows an array of four half-wave dipole antennas placed on a circle of radius $a = \lambda/4$. The elements are identical with radius $\lambda/200$. The radiation pattern of such an array can be found easily using pattern multiplication method which is discussed in detail in Sec. 2.5. The element pattern of a half-wave dipole antenna in the H-plane is a unit circle. Since the total pattern is the product of the element pattern and array factor, we can say that total pattern is simply equal to the array factor in this case. The setup for the array factor can be seen in Fig. 1.2 where $\theta = 90°$ and the xy-plane can be seen with φ starting from the x-axis. The elements (P_1, P_2, P_3 and P_4) are assumed to be excited with voltages $V_1 = 1\angle 0°$, $V_2 = 1\angle 30°$, $V_3 = 1\angle 60°$, and $V_4 = 1\angle 90°$, respectively.
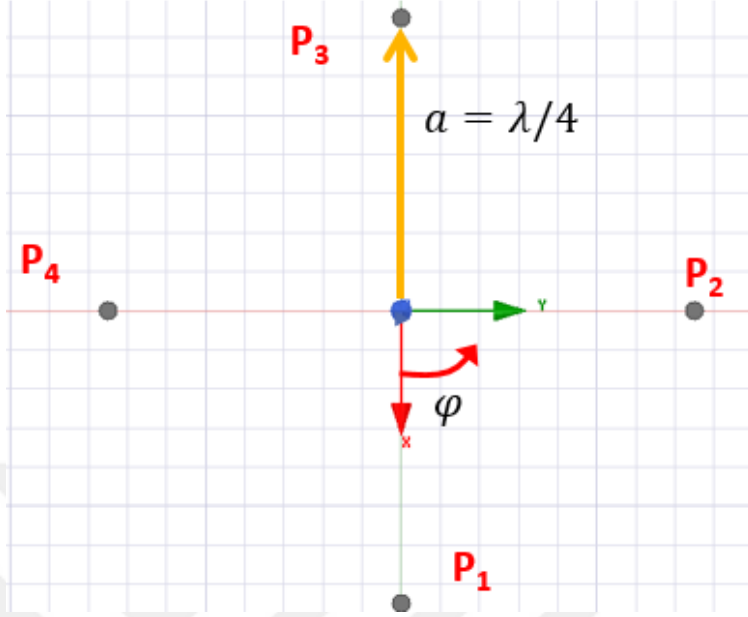
Figure 1.2: Four isotropic sources arranged in a circular array.

Then the array factor can be expressed as follows

$$AF = \sum_{n=1}^{4} V_n e^{j\beta \widehat{\mathbf{r}} \cdot \mathbf{r_n'}} \tag{1.1}$$

where $\widehat{\mathbf{r}}$ is the position vector from the origin to the field point and $\mathbf{r_n'}$ is the vector from the origin to the source point. They are defined as

$$\widehat{\mathbf{r}} = x\widehat{\mathbf{x}} + y\widehat{\mathbf{y}} + z\widehat{\mathbf{z}} = \sin\theta\cos\varphi\widehat{\mathbf{x}} + \sin\theta\sin\varphi\widehat{\mathbf{y}} + \cos\theta\widehat{\mathbf{z}}$$
$$\mathbf{r_n'} = x_n\widehat{\mathbf{x}} + y_n\widehat{\mathbf{y}} = a\cos\varphi_n\widehat{\mathbf{x}} + a\sin\varphi_n\widehat{\mathbf{y}}$$

for the spherical co-ordinate system. Then the array factor is simply given by

$$AF = \sum_{n=1}^{4} V_n e^{j\beta(x_n \sin\theta\cos\varphi + y_n \sin\theta\sin\varphi)} \tag{1.2}$$

5
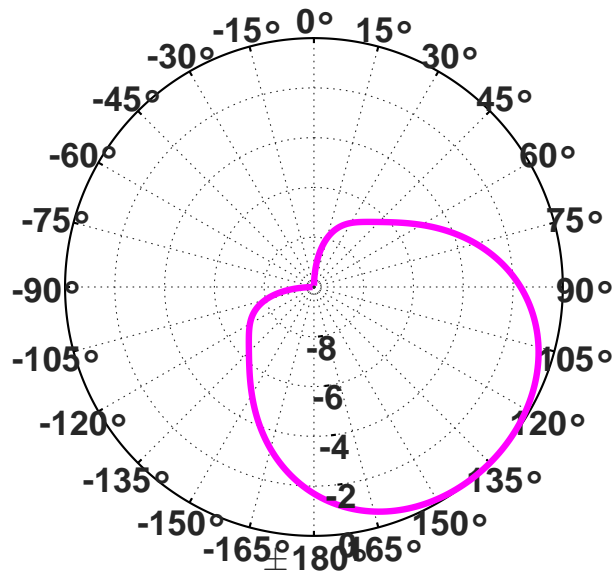
Figure 1.3: Theoretical pattern of the circular array of four dipoles calculated by pattern multiplication method.

Fig. 1.3 shows the resultant pattern after plotting Eq. 1.2. This is the total radiation pattern of the circular array of four dipoles calculated theoretically since element pattern in H-plane is a unit circle. It must be noted that this method does not take into account the effects of mutual coupling. In reality the practical pattern is very different from the theoretical pattern because of mutual coupling. The same antennas when excited with the same voltages gives the pattern as shown in Fig. 1.4.
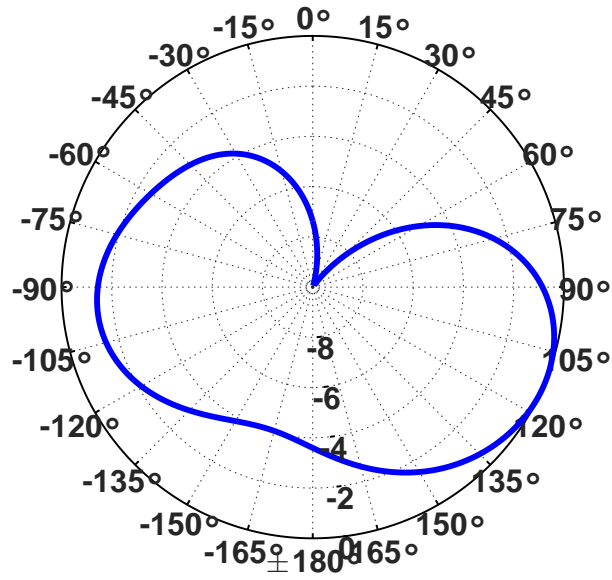
Figure 1.4: The real practical pattern of circular array of four dipoles.

It can be seen that the theoretical pattern and practical pattern are totally different from one another because of mutual coupling. When the same antenna is excited by $V_1' = 0.29\angle 83°$, $V_2' = 0.23\angle 94°$, $V_3' = 0.16\angle 136°$ and $V_4' = 0.056\angle 177°$ respectively, the following pattern is achieved as shown in Fig. 1.5.
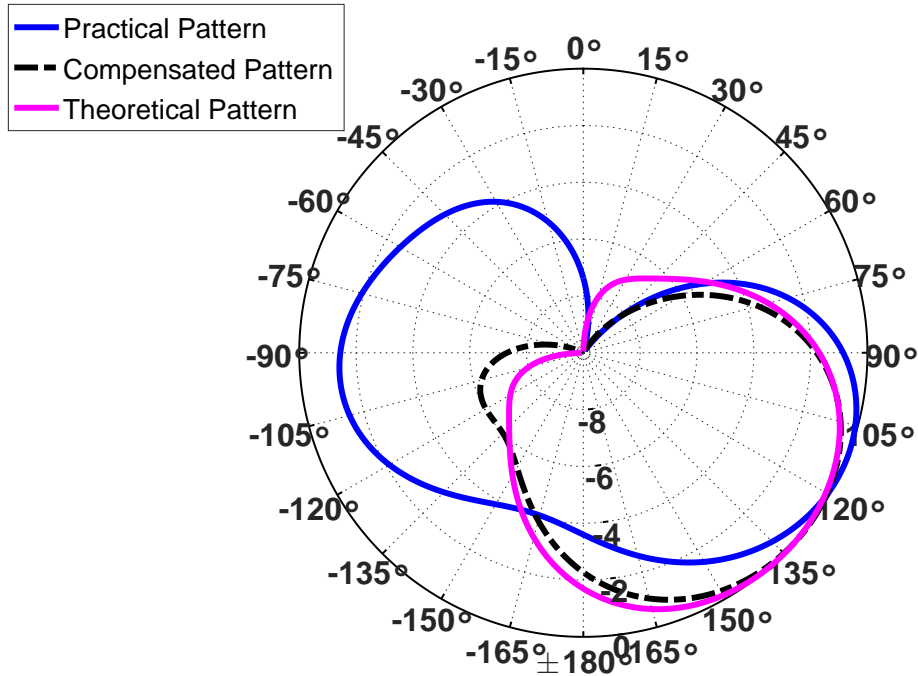
Figure 1.5: Radiation pattern of a circular array of four dipoles.

The black curve in Fig. 1.5 is the radiation pattern of the same circular array in the presence of mutual coupling excited by these new voltages. It can be seen that this black pattern is very similar to the theoretical pattern in pink. This is called the compensated pattern which has been obtained after the compensation of mutual coupling in the circular array. The situation shown in Fig. 1.5 is the main motivation behind this dissertation. The purpose of this work is to compute the so called compensated voltages for an array of thin wire antennas. In this work we use method of moment [11] to compute the mutual impedance between the array elements which are then used to compute the compensated voltages. The details are given in Section 2.6.

1.2 Approach

The intent of this study is to numerically compensate for mutual coupling using method of moment in small arrays in different configurations. The compensation is performed for linear and circular arrays both in 2-D and 3-D. A Matlab code (henceforth algorithm) is written to numerically compute the far-field radiation patterns for thin wire antennas using

MoM. Piecewise sinusoidal (PWS) functions are used as expansion functions. Testing is performed using Galerkin method. The moment matrix [11] is computed by a closed form of the integral in Appendix B using the Si and Ci functions [2]. From the moment matrix and its inverse Z, Y, and S parameters for the array can be computed. A magnetic frill current [12] is used for the excitation of the individual antenna element as shown in Appendix C. The radiation pattern computed using MoM is calculated in the presence of mutual coupling. The S parameters are used for calculating the new compensated voltages. When the array is excited with these new compensated voltages the radiation pattern is the compensated pattern where the effect of mutual coupling has been reduced. The result is compared with the theoretical pattern calculated using the pattern multiplication method since it does not take into account the mutual coupling. When perfect mutual compensation has been achieved, the theoretical pattern and compensated pattern should be exactly the same, otherwise the two patterns will differ. The computed compensated radiation patterns for the 2-D and 3-D arrays have been verified using ANSYS® HFSS™ software.

1.3   Overview

This work analyzes thin wire dipole arrays with identical and non-identical elements using method of moments and then compensate for the mutual coupling between the array elements. The organization of the thesis is as following.

Chapter 2 gives a brief background of the different computational electromagnetic methods for low and high frequencies. A single thin wire antenna is analyzed using MoM in free space which is further extended to an array of thin wire dipoles. Finally, the compensation method has been discussed which is derived using the scattering matrix.

Chapter 3, presents the simulation results. First, mutual impedances have been shown for identical and non-identical arrays in different configurations, i.e., co-linear, staggered, and non-staggered. The simulated results are compared with theoretical results [1], [13]. Next, the compensation technique is applied to the above array configurations and the results are compared with those of pattern multiplication. In case of non-identical arrays, the array factor is calculated by summing the isolated pattern of each wire antenna in the array. Compensation has been shown for planar arrays and compared with [14] and [15]. Circular and 3-D arrays compensation are shown and compared with the results from ANSYS® HFSS™ software simulations.

Finally, Chapter 4 concludes this thesis with a summary of the main findings and suggestions for future work.

Chapter 2

Methods of Computational Electromagnetics (CEM)

Numerical methods have been used extensively to speed up antenna computations. Nowadays, plenty of commercial softwares are available but due to their high cost and complex nature they may not be the best choice for researchers. The simulations using these commercial softwares may last for days and months depending on the complexity of the geometry even with the most high-end CPUs. Hence, for a specific complex problem developing a source code to efficiently calculate an approximate solution using FORTRAN® or MATLAB®, maybe more feasible in terms of cost and time.

While the data gathered from the experimental measurements can be useful, the process itself can be extremely expensive in terms of time and money. On the other hand, the CEM algorithms can help simulate a variety of problems in much shorter time. Many design parameters can be varied and its effect can be analyzed before actually building the real system. CEM can help the designer in better visualization of the problem with computer aided designs.

Due to the broad range of electromagnetic (EM) problems, many numerical methods have been developed. These numerical techniques can be divided into two broad classes. Full-wave methods (also known as low frequency and/or exact methods) and High-Frequency methods (also known as approximate methods).

Because of computational resources the full-wave methods are mostly limited to problems

which are not very large electrically. The computational domain, which includes the antenna and/or scatterer, is first discretized and then a matrix equation of the form $[A][x] = [B]$ with solution of $x = [A^{-1}][B]$ is generated. Whereas, the high frequency methods are used for electrically large problems.

Maxwell's equations exist in both differential and integral form, hence the full-wave problems can be solved with Partial Differential Equations (PDEs) or Integral Equations (IEs). The PDE technique divides the antenna/scatterer and the space surrounding it into small segments. Due to computational limitations the surrounding space can not be infinite, therefore, some absorbing boundary conditions (ABC) must be introduced around the antenna/scatter to simulate infinite space [16].

On the other hand, IE technique subdivides the antenna/scatterer into small segments but not the surrounding space. Equivalence theorem is used to produce equivalent currents, where required, which radiate in free space. The three different types of integral equations are, Electric Field Integral Equation (EFIE), Magnetic Field Integral Equation (MFIE), and Combined Field Integral Equation (CFIE).

Under IE and PDE techniques problems can be divided into time domain and frequency domain. Frequency domain solves the Maxwell's equation at a single frequency, which makes it a suitable candidate for solving problems with narrow bandwidths. The time domain on the other hand, calculates the system response to a time limited pulse of appropriate shape, which makes it a relatively better technique for wide bandwidth problems. The CEM techniques, as mentioned above, can be divided into different groups as shown in the Fig. 2.1.
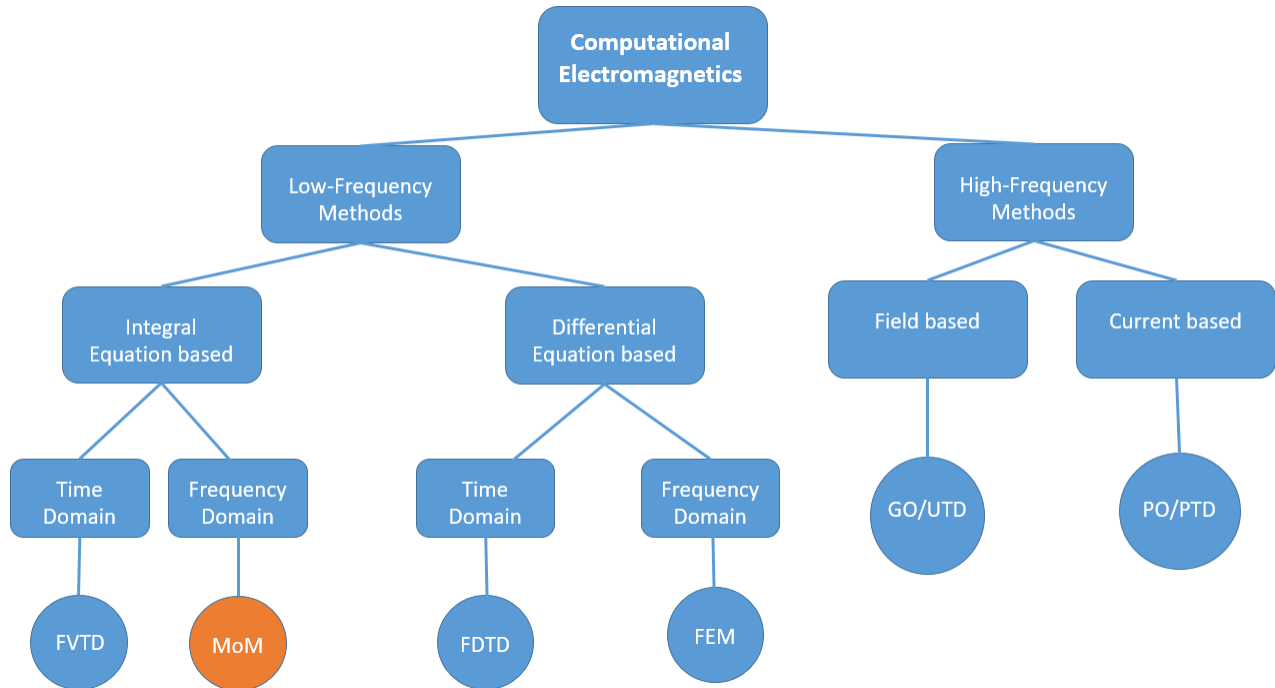
Figure 2.1: A flow chart showing different computational electromagnetic techniques.

2.1 Low-Frequency Methods

Low-frequency methods solve problems that are usually electrically small due to limitations of computational and time resources. The methods included in this sub-group of the CEM techniques are briefly mentioned below.

2.1.1 Finite Difference Time Domain Method

The Finite Difference Time Domain (FDTD) method is a well known technique for solving electromagnetic problems. It can be applied to a variety of problems such as, scattering from dielectrics, metal objects, antennas, and electromagnetic absorption in human body when exposed to EM radiations. The method is simple and easy to implement even in programming.

FDTD solves Maxwell's equations in the time domain by discretizing the solution workspace into small elements. The electric and magnetic fields are computed from one another in a 'leap-frog' manner. Despite high memory requirements this method excels in

the analysis of inhomogeneous and nonlinear media. The memory requirement is high due to discretization of the entire solution space. In addition to this, FDTD suffers from the dispersion issues and the need to truncate the solution boundary. This time domain method has a wide variety of applications ranging from packaging and waveguide problems, and the study of wave propagation in complex dielectrics.

2.1.2 Finite Element Method

The Finite Element Method (FEM) is used to solve frequency domain boundary valued electromagnetic problems. Canonical elements of differing shapes are used which allows for a highly accurate discretization of the solution domain. The solution domain needs to be truncated in FEM similar to the FDTD case, which limits its use for radiation and scattering problems unless a boundary integral equation approach is used.

2.1.3 Method of Moments

The Method of Moments is one of the first full-wave numerical method used for solving electromagnetic radiation and scattering problems [11]. It is used to solve electromagnetic boundary or volume integral equations in the frequency domain. It models the problem with an exact equation usually an integral equation then solves it numerically/ approximately. As the electromagnetic sources are the quantities of interest, MoM is very useful in solving radiation and scattering problems. It is considered to be the best method when metallic objects and wires are of interest. This method is explained in more detail in Section 2.3.

2.2 High-Frequency Methods

Even prior to the birth of super computers, large scale problems existed, which were difficult to solve. For example calculation of an antenna's radiation pattern when mounted on a large structure or radar cross section of an electrically large target. For electrically large problems asymptotic methods produce accurate results and at times these initial results can be passed on to other computationally demanding methods if further accuracy is required. Some of the high-frequency methods are briefly introduced below.

2.2.1 Uniform Theory of Diffraction (UTD)

UTD utilizes ray-optics to determine EM wave propagation. It takes into account the fields diffracted from the edges. The method is fast but does not produce accurate results for complex structures.

2.2.2 Geometrical Optics (GO)

This method is used to approximate high-frequency surface currents which allows boundary integration to obtain the fields. GO does not account for the diffracted fields from the edges and the multiple reflections, thus some corrections have to be added to it. GO can be used in reflector antenna analyses and radar cross section prediction codes.

2.2.3 Physical Theory of Diffraction (PTD)

This method is mostly used in radar cross section and scattering analyses. PTD aids the GO solution by adding the effects of non-uniform currents at the diffracting edges of an object.

2.3 The Method of Moments

The basic approach used in this frequency domain method is to expand an unknown function in terms of known functions with unknown coefficients. This method usually starts with an exact linear operator equation and solves it approximately. On the other hand, FDTD approximates the differential equation with a difference equation and solves it exactly. In both cases the computed result is an approximation to the exact result. This process can be formally introduced as the method of weighted residuals known as the method of moments. Given the operator equation,

$$L(f) = g \tag{2.1}$$

where L is a linear operator, g is a known function, and f is unknown. In case of electromagnetics L is an integro-differential operator, f is the unknown function (current, charge) and g is a known excitation source (incident field). f can be expanded into a sum of N weighted *basis or expansion functions*,

$$f = \sum_{n=1}^{N} \alpha_n h_n(x) \tag{2.2}$$

where $h_n(x)$ is the expansion function and α_n is the expansion coefficient. After substituting (2.2) in (2.1), we have the following,

$$L\left(\sum_{n=1}^{N} \alpha_n h_n(x)\right) = g \tag{2.3}$$

Since L is a linear operator, (2.3) can be written as

$$\sum_{n=1}^{N} \alpha_n L(h_n(x)) = g \tag{2.4}$$

Equation (2.4) is tested by defining a set of testing (weighting) functions $w_m(x)$,

$$\left\langle w_m, \sum_{n=1}^{N} \alpha_n L(h_n(x)) \right\rangle = <w_m, g> \quad \text{where} \quad m = 1, 2, \ldots, N. \tag{2.5}$$

The bracket $<>$ stands for the defined inner product which is used in the testing process. Equation (2.5) can be written as N separate equations:

$$<w_1, \alpha_1 L(h_1(x))> + <w_1, \alpha_2 L(h_2(x))> + \cdots + <w_1, \alpha_N L(h_N(x))> = <w_1, g> \tag{2.6a}$$

$$<w_2, \alpha_1 L(h_1(x))> + <w_2, \alpha_2 L(h_2(x))> + \cdots + <w_2, \alpha_N L(h_N(x))> = <w_2, g> \tag{2.6b}$$

$$\vdots$$

$$<w_N, \alpha_1 L(h_1(x))> + <w_N, \alpha_2 L(h_2(x))> + \cdots + <w_N, \alpha_N L(h_N(x))> = <w_N, g> \tag{2.6c}$$

The above N equations in N unknowns can be written in matrix form as :

$$\begin{bmatrix} Z_{11} & Z_{12} & \ldots & Z_{1N} \\ Z_{21} & Z_{22} & \ldots & Z_{2N} \\ \vdots & \vdots & \vdots & \vdots \\ Z_{m1} & \ldots & Z_{mn} & Z_{mN} \\ \vdots & & & \\ Z_{N1} & Z_{N2} & \ldots & Z_{NN} \end{bmatrix} \begin{bmatrix} \alpha_1 \\ \alpha_2 \\ \vdots \\ \alpha_m \\ \vdots \\ \alpha_N \end{bmatrix} = \begin{bmatrix} g_1 \\ g_2 \\ \vdots \\ g_m \\ \vdots \\ g_N \end{bmatrix} \tag{2.7}$$

Where,

$$Z_{mn} = <w_m, L(h_n(x))> \tag{2.8}$$

16

and

$$g_m = < w_m, g(x) >$$
(2.9)

Then the unknown expansion coefficients can be calculated by taking the inverse of the moment matrix, as shown below,

$$
\begin{bmatrix} \alpha_1 \\ \alpha_2 \\ \vdots \\ \alpha_N \end{bmatrix} =
\begin{bmatrix} Z_{11} & \dots & Z_{1N} \\ \vdots & & \vdots \\ \vdots & & \vdots \\ Z_{N1} & \dots & Z_{NN} \end{bmatrix}^{-1}
\begin{bmatrix} g_1 \\ g_2 \\ \vdots \\ g_N \end{bmatrix}
$$
(2.10)

If the weighting function is $w_m(x) = \delta(x - x_m)$, then the testing method is called *point-matching*, whereas for $w_m(x) = h_m(x)$, it is called *Galerkin's Method* [1].

2.4 Dipoles

Wire antennas are one of the most popular antennas that are still an integral part of our technological society due to its infallible characteristics. They are inexpensive, robust and simple to understand and use. Due to these features, it is one of the most widely researched antenna since it can be used as a building block for developing other complex antennas.

2.4.1 Single Dipole in Free Space

The ideal Hertzian dipole is the fundamental building block of a practical dipole. The ideal dipole can be defined as an infinitesimal element with a uniform current magnitude and phase. Therefore, we can assume that a dipole of any length can be approximated as the vector sum of the contributions from all the ideal dipoles weighted by the current distributions. The far-field pattern of a z-directed dipole in an array is called the element pattern (EP), which is $\sin \theta$ for the Hertzian dipole. When the length of the dipole is finite the current and phase are no longer constant. Dipoles that have $L \leqslant \lambda/2$ are known as *single mode* antennas. The current distribution may change in magnitude or phase but not in shape. Similarly, a short dipole whose length $L << \lambda/2$ the amplitude can be approximated by a triangle where as the current is in phase. In case of a half-wave dipole, the amplitude is sinusoidal with current in phase. The exact expression for the radiation pattern of a

half-wave dipole (assuming zero radius) is given by

$$F(\theta) = \frac{\cos\left[(\pi/2)\cos\theta\right]}{\sin\theta} \tag{2.11}$$

For these dipoles, the radiation pattern will be strongest along the normal and weakest along the axis of the dipole as shown in Fig. 2.2.
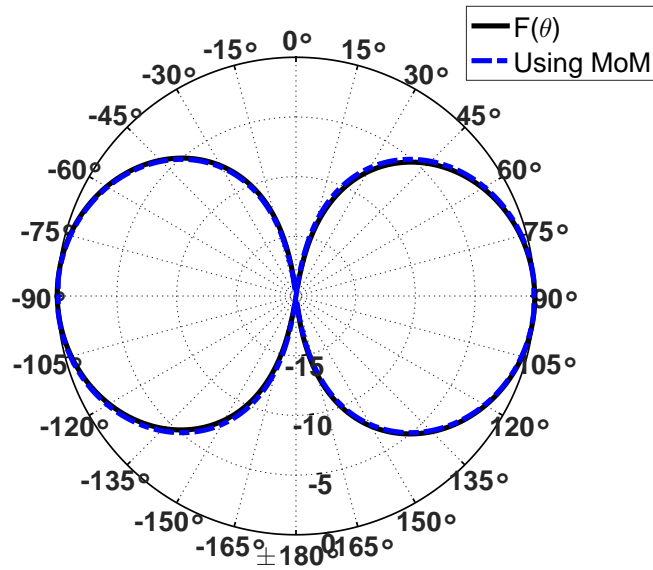
Figure 2.2: Normalized E-plane pattern of a half-wave dipole.

The half-wave dipole is omni-directional in H-plane as shown in Fig. 2.3.
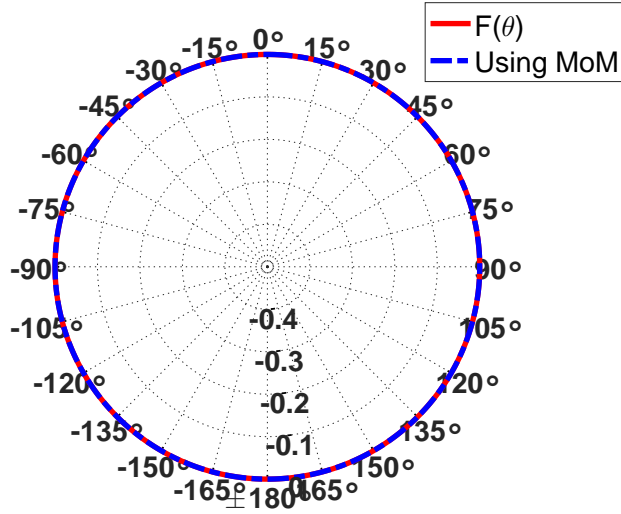
Figure 2.3: Normalized H-plane pattern of a half-wave dipole.

The above figures show that the radiation pattern plotted due to the exact Eq. 2.11 which assumes zero radius is approximately equal to the numerical pattern computed using method of moments which assumes a finite radius $\lambda/1000$. This close approximation shows us the accuracy of the numerical method used. The short dipole or ideal dipole has a half-power beamwidth of $90°$ which is decreased to $78°$ in the case of the half-wave dipole. For dipoles longer than one wavelength, the currents on the antenna are out of phase on some sections with the others, which results in partial or total cancellation in the far-fields. The Appendix A gives the details of application of MoM to thin wire antennas. Using this method, a sample calculation of the current and phase is shown in Fig. 2.4, for a wire of length 0.4781λ, radius $\lambda/1000$, and number of expansion functions $NP = 63$. An input impedance of $Z_{in} = 73.7210 + 5.3596i$ Ω was calculated which suggests that the radiation resistance is 73.7 Ω.
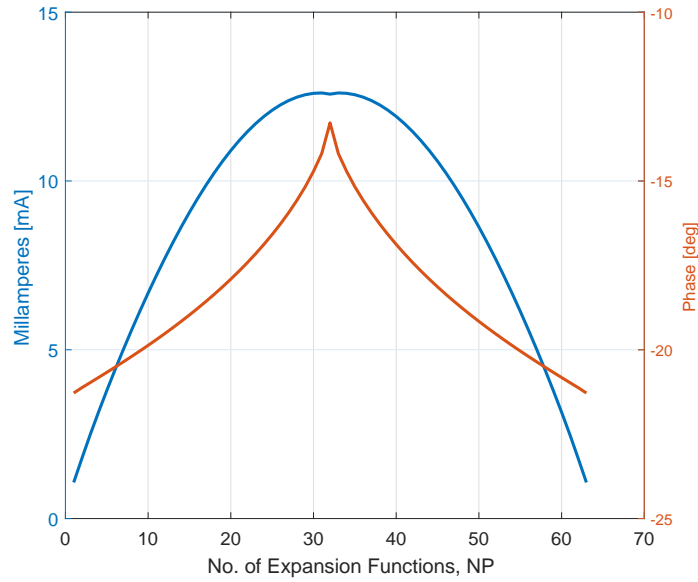
Figure 2.4: Magnitude and phase of the current distribution for a center-fed dipole in free space with length $L = 0.4781\lambda$, radius $a = \lambda/1000$ and number of expansion functions $NP = 63$.

The impedance is inductive in this case due to the imaginary part which can be made totally resistive by shortening the dipole length. For dipoles with lengths $\lambda/2$ and below, the radiation resistance decreases monotonically with length and is almost independent of diameter, whereas the reactive component depends heavily on diameter. The thinner antennas are more capacitive for a given length. In practice, a dipole has a finite length-to-diameter ratio. Additionally, the environment surrounding the antenna also affects its impedance. Both the radiation pattern and impedance are influenced by the presence of nearby objects.

2.5 Array Theory

Principle of pattern multiplication states that the radiation pattern of an array is the product of the pattern of the individual antenna with the array pattern. The array pattern is a function of the location of the antennas in the original array and their relative complex excitation amplitudes. Array factor is the pattern of the array with actual elements replaced by isotropic point sources. The total pattern of the array is then the product of the element pattern and array factor.

$$\text{Total Pattern} = \text{Element pattern x Array pattern}$$

20
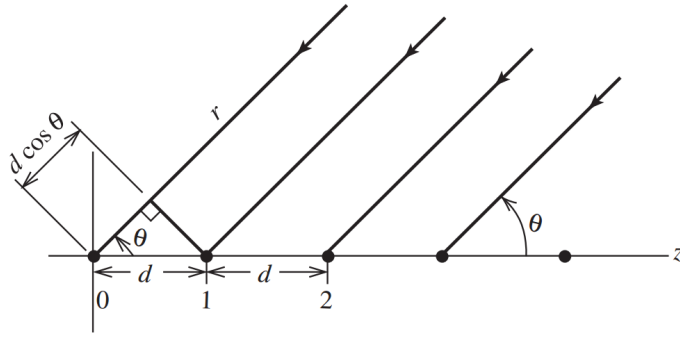
Figure 2.5: Equally spaced linear array of isotropic point sources [1].

Consider a linear array of dipoles with elements equally spaced along the z-axis. In order to calculate the array factor for such an array the elements of the array are replaced by isotropic point sources which are placed at the center of these elements as shown in Fig. 2.5. These point sources respond equally in all directions to an incoming plane wave. The point source at origin has a zero phase for convenience. The corresponding phase of waves at element 1 relative to the origin is $\beta d \cos \theta$ which is the spatial phase delay. Similarly, the phase at each corresponding element on the right is less than its nearest neighbor on the left. In other words, the wave will first hit the nth element and lastly the element at the origin [1].

$$AF = I_0 + I_1 e^{j\beta d \cos \theta} + I_2 e^{j\beta 2d \cos \theta} + \cdots = \sum_{n=0}^{N-1} I_n e^{j\beta nd \cos \theta} \qquad (2.12)$$

In the case of short dipole the element pattern is simply $\sin \theta$ in the E-plane which is similar to that in Fig. 2.2. Since we are using single mode antennas the element pattern can be taken as $\sin \theta$ in E-plane and a unit circle in the H-plane similar to Fig. 2.3. Pattern multiplication has the advantage of giving us a quick sketch of the pattern by just knowing the pattern of an isolated element and array pattern but it does not consider mutual coupling between the array elements. The limitation of pattern multiplication is that all the elements of the array must be identical. Hence, we can use pattern multiplication as a reference for comparing when the mutual coupling has been compensated for an array of identical elements. The compensated far-field pattern must be similar to that of pattern multiplication method. In case of non-identical elements, e.g., when the length or radius of the elements are different in the array then the conventional method of pattern multiplication does not apply. In that case, the array factor method could be redefined as simply taking the isolated individual patterns of each element and then adding it up. This will give the complete pattern of the

21

array without mutual coupling which can be used as a reference for comparing with the patterns that have been mutually compensated.

2.6 Compensation Method

Consider an array of N thin wire antennas as shown in Fig. 2.6. The pattern of this array can be changed by fixing the input current I_n of the nth element of the array. These input currents without mutual coupling can be found as,

$$I_n = \frac{V_{gn}}{Z_0 + Z_n} \quad \text{for n=1,2..N.} \tag{2.13}$$

Here V_{gn} is the generator voltage feeding the nth antenna, $Z_0 = 50 \ \Omega$ is the characteristic impedance of the transmission line (of zero length), which is equal to the internal resistance of the source Z_g, and Z_n is the input impedance of the nth antenna when it is isolated, that is, when the other N-1 antennas are removed.
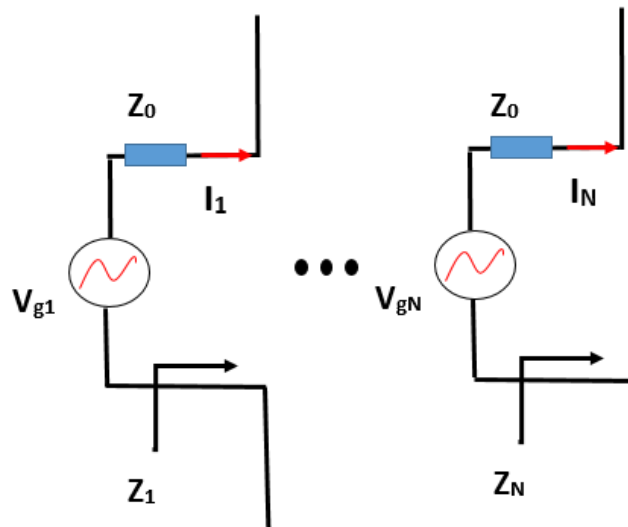
Figure 2.6: Equivalent circuit of N antennas with no mutual coupling

Figure 2.6 shows the equivalent circuit. When mutual coupling exists, the input impedance of each individual antenna changes to Z_n', thus changing the input currents which would change the radiation pattern of the element. Note that two isolated identical antennas must have same impedance $Z_m = Z_n$. This however does not imply that input impedance of these antennas in the array will also be the same $(Z_m' \neq Z_n')$, in general. In order to bring

22

the currents back to the desired values I_n, the generator voltages must be readjusted to V'_{gn}. The input impedance has changed from Z_n to Z'_n whereas the input currents must remain the same as shown in Fig. 2.7. Our problem is to find these adjusted voltage source values V'_{gn} to give the desired currents I_n in the presence of mutual coupling.
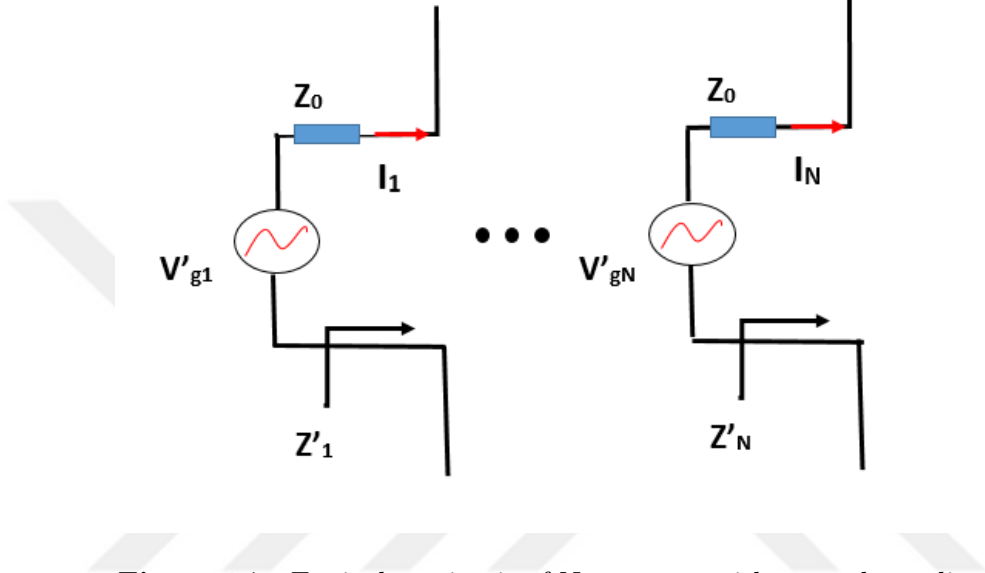
Figure 2.7: Equivalent circuit of N antennas with mutual coupling

Thus the source voltages are changed from V_{gn} to V'_{gn}. The desired current can be written as,

$$I_n = \frac{V'_{gn}}{Z_0 + Z'_n} \tag{2.14}$$

Here both Z'_n and V'_{gn} are unknown. However, Z'_n can be calculated using MoM.

Using transmission line theory, we know that the current can be expressed as,

$$I_n = \frac{V_n^+ - V_n^-}{Z_0} \tag{2.15}$$

where V_n^+ is the forward (incident) voltage entering the nth antenna of the N-port network defined by,

$$V_n^+ = \frac{V'_{gn}}{2} \tag{2.16}$$

and V_n^- is the reflected voltage from the n_{th} antenna. It can be written as,

$$
\begin{aligned}
V_n^- &= S_{n1}V_1^+ + S_{n2}V_2^+ + \cdots + S_{nN}V_N^+ \\
&= (S_{n1}V_{g1}' + S_{n2}V_{g2}' + \cdots + S_{nN}V_{gN}')/2
\end{aligned}
\tag{2.17}
$$

Where, S_{ij} is the element of the scattering matrix for the system. Substituting the values of (2.16) and (2.17) in (2.15) we get

$$
\begin{aligned}
I_1 &= (V_1^+ - V_1^-)/Z_0 \\
&= V_{g1}'/(2Z_0) - (1/Z_0)\{S_{11}V_1^+ + S_{12}V_2^+ + \cdots + S_{1N}V_N^+\} \\
&= 1/(2Z_0)\{V_{g1}' - S_{11}V_{g1}' - S_{12}V_{g2}' - \cdots - S_{1N}V_{gN}'\} ,
\end{aligned}
\tag{2.18}
$$

$$
I_2 = 1/(2Z_0)\{V_{g2}' - S_{12}V_{g1}' - S_{22}V_{g2}' - \cdots - S_{2N}V_{gN}'\} ,
\tag{2.19}
$$

$$
I_N = 1/(2Z_0)\{V_{gN}' - S_{N1}V_{g1}' - S_{N2}V_{g2}' - \cdots - S_{NN}V_{gN}'\} .
\tag{2.20}
$$

The above equations can be written in matrix form as

$$
\begin{bmatrix} I_1 \\ I_2 \\ \vdots \\ I_N \end{bmatrix} = \frac{1}{2Z_0} \begin{bmatrix} V_{g1}' \\ V_{g2}' \\ \vdots \\ V_{gN}' \end{bmatrix} - \frac{1}{2Z_0} \begin{bmatrix} S_{11} & S_{12} & \cdots & S_{1N} \\ S_{21} & S_{22} & \cdots & S_{2N} \\ \vdots & \vdots & \vdots & \vdots \\ S_{N1} & S_{N2} & \cdots & S_{NN} \end{bmatrix} \begin{bmatrix} V_{g1}' \\ V_{g2}' \\ \vdots \\ V_{gN}' \end{bmatrix}
$$

Or in short hand notation as

$$
[I] = \frac{1}{2Z_0}\{U - S\}[V_g']
\tag{2.21}
$$

Here [I] is the $N \times 1$ column vector of the desired input currents. U is $N \times N$ unit matrix and $[Vg']$ is the $N \times 1$ column vector of the desired compensated source voltages feeding the antennas. The desired compensated source voltages (in the presence of mutual coupling) are given by,

$$
[V_g'] = (2Z_0)\{U - S\}^{-1}[I]
\tag{2.22}
$$

Or

$$
[V_g'] = (2Z_0)\{U - S\}^{-1} \begin{bmatrix} \frac{V_{g1}}{Z_0 + Z_1} \\ \frac{V_{g2}}{Z_0 + Z_2} \\ \vdots \\ \frac{V_{gN}}{Z_0 + Z_N} \end{bmatrix}
$$

24

2.7 Formulation of Matlab Code

In order to solve the currents on the wire antennas, MoM using the Galerkin's method has been applied. This means, the basis function and testing function are the same, which are the PWS functions defined by (A.8) in the Appendix. Using (2.10), we define α as the coefficients of the expansion functions of the unknown currents on the wires in the array, Z matrix as the moment matrix and g matrix is the excitation or voltage matrix.

The Z matrix is the moment matrix which is found using (B.1) in the Appendix. Equation (B.1) may be evaluated without difficulty by numerical integration. However, when $\rho = a$ and a is small (i.e., wires of very small radius) it may be preferable to carry out the integration in the form of sine "Si" and cosine "Ci" integrals given in (B.4) and (B.5). The elements of Z_{mn} are given by $Z_{mn} = R_{mn} + jX_{mn}$, which are defined in the closed form equations given by (B.6) and (B.7). This calculates the moment matrix for the arrays of wires.

The wires are center fed and the voltage source used for the wires is modelled using magnetic frill current given by (C.5). Once the moment matrix, Z, and voltage matrix, V, are known we can calculate the current matrix, I, for the array. Using this the radiation pattern for the array in the presence of mutual coupling can be computed. This pattern is the real life practical pattern of the array. Using the moment matrix and its inverse one can compute the open circuit parameters matrix Z_o, and the short circuit parameters Y_s matrix, and scattering matrix S for the array. The compensated current is calculated by,

$$I_{compensated} = [Z^{-1}][V_g']\qquad(2.23)$$

This current produces the radiation pattern when the mutual coupling has been compensated for. This new compensated radiation pattern is then compared with the theoretical pattern obtained using principle of pattern multiplication. In the following we plot three patterns: (i) *uncompensated voltages* (this pattern is produced by the original voltages in the presence of mutual coupling. (ii) *compensated voltages* (this pattern is computed using the compensated voltages in the presence of mutual coupling), and (iii) *pattern multiplication method* (this pattern is computed using the original voltages and without mutual coupling). Chapter 3 shows comparison of the above three mentioned patterns for different antenna orientations.

Chapter 3

Simulations and Results

Simulation results are divided into two sections, identical and non-identical arrays. For each section the mutual impedance has been calculated and then the far-field patterns are shown.

3.1 Identical Arrays

Two element identical arrays are presented in this section. Length of a single element is $L = 0.4781\lambda$ and radius $a = \lambda/1000$. The number of expansion functions (NP) used for each dipole are thirty one. The elements are arranged in three different configurations:

- Non-staggered (parallel)

- Staggered

- Collinear

3.1.1 Mutual Impedance

The mutual impedance for two element identical arrays is calculated in this section. These results have been calculated in the literature before [2]. They have been regenerated in order to confirm the proper working of the algorithm.

3.1.1.1 Non Staggered
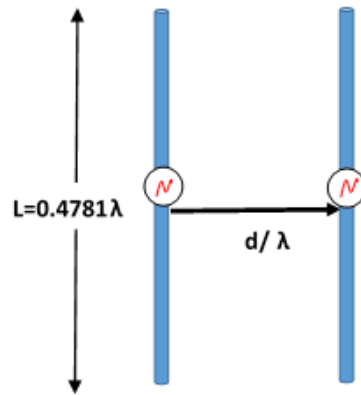
Figure 3.1: Two parallel dipole antennas in non-staggered arrangement with length $L = 0.4781\lambda$, radius $a = 0.001\lambda$, separation d/λ, and $\lambda = 1$ m.
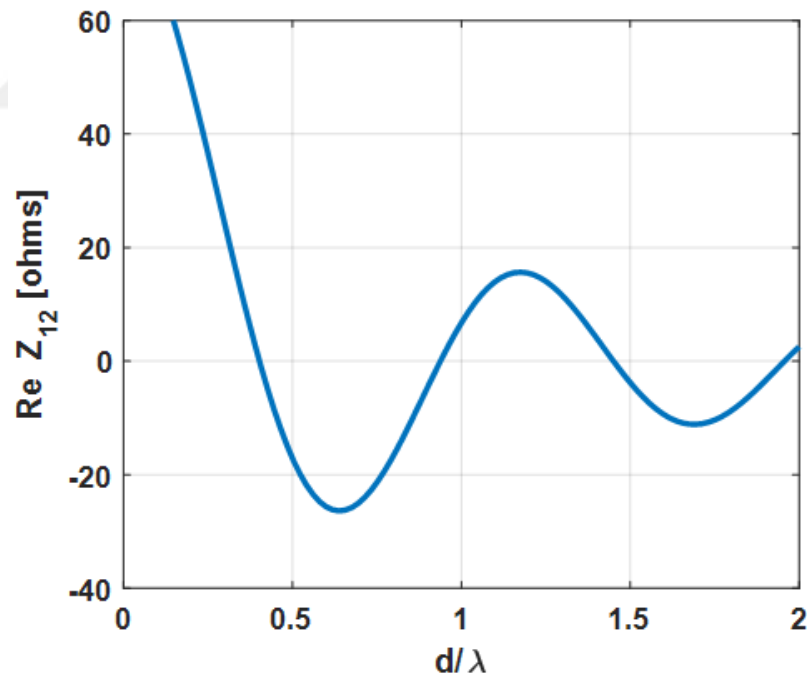
Figure 3.2: Real part of mutual impedance between two parallel dipole antennas as a function of spacing relative to wavelength with $L = 0.4781\lambda$ and $a = 0.001\lambda$. Geometry shown in Fig. 3.1

.
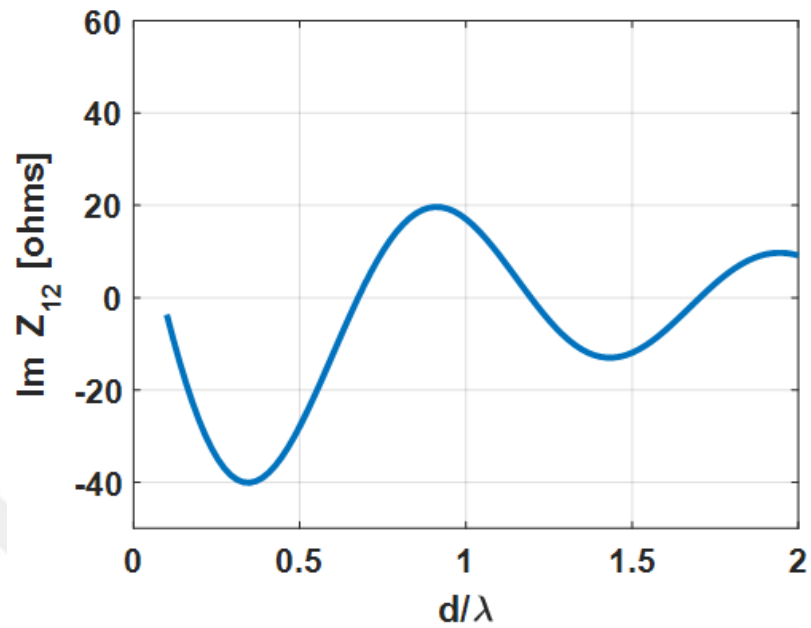
Figure 3.3: Imaginary part of mutual impedance between two parallel dipole antennas as a function of spacing relative to wavelength with $L = 0.4781\lambda$ and $a = 0.001\lambda$. Geometry shown in Fig. 3.1.

Figs. 3.2 and 3.3 are in conformation with those presented in [2].

3.1.1.2 Staggered
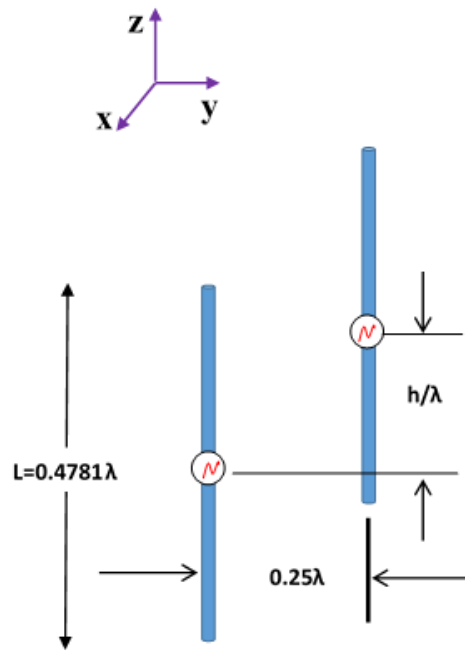
Figure 3.4: Two identical parallel dipole antennas in staggered arrangement with length $L = 0.4781\lambda$, radius $a = 0.001\lambda$, fixed horizontal separation of 0.25λ, and staggered by h/λ.

The mutual impedance between two staggered dipole antennas, as a function of spacing relative to wavelength, which were computed by [2], were removed from the later editions of the book due to ambiguity in the results. The correct results for this case are presented below in Figs. 3.5 and 3.6.
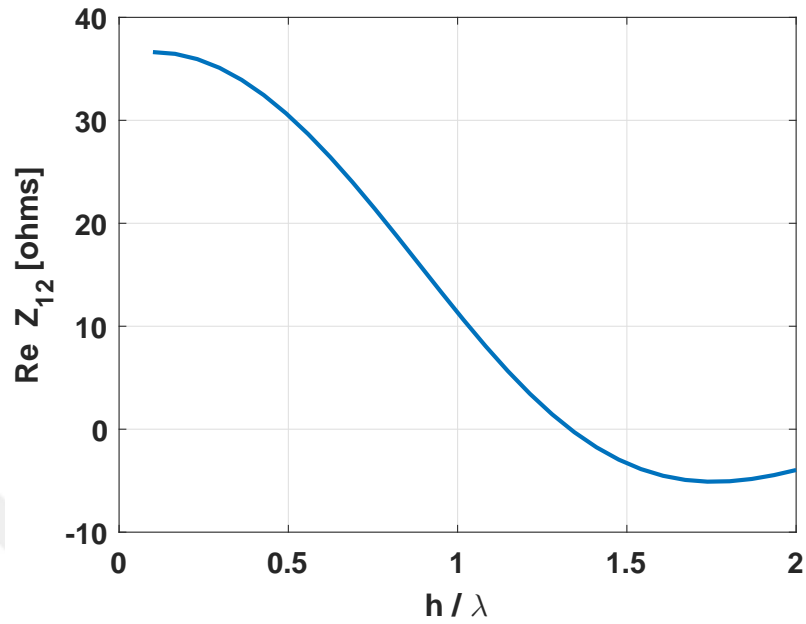
Figure 3.5: Real part of mutual impedance between two identical but staggered dipole antennas of length $L = 0.4781\lambda$, radius $a = 0.001\lambda$, fixed horizontal separation of 0.25λ, and staggered by h/λ.
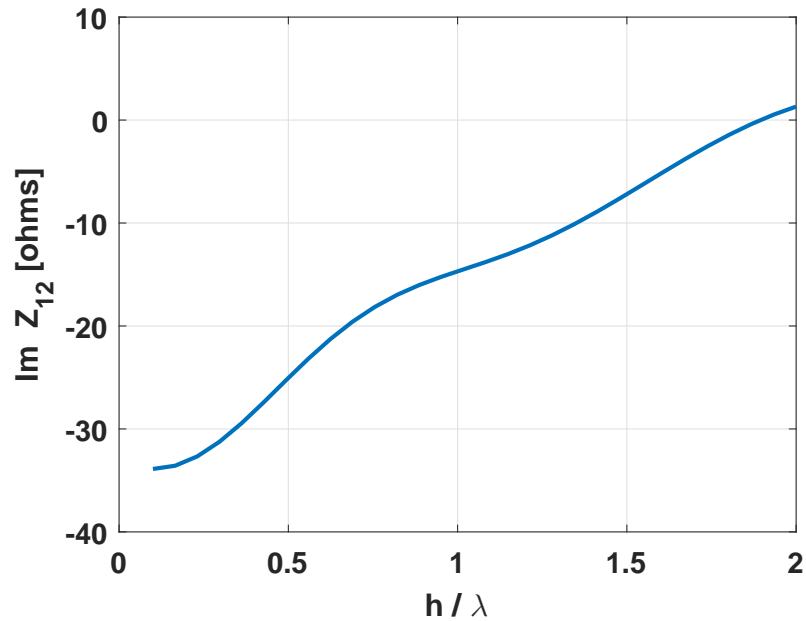
Figure 3.6: Imaginary part of mutual impedance between two identical but staggered dipole antennas of length $L = 0.4781\lambda$, radius $a = 0.001\lambda$, fixed horizontal separation of 0.25λ, and staggered by h/λ.

30

It can be noted easily when $h/\lambda = 0$, the case is similar to that of non-staggered antenna and by examining the mutual impedance at $d/\lambda = 0.25$, the value of Fig. 3.2 matches with that of Fig. 3.5. Similarly, the same holds true for Fig. 3.3 and Fig. 3.6, which also verifies the authenticity of the results. These results were also verified with [13].

3.1.1.3 Collinear
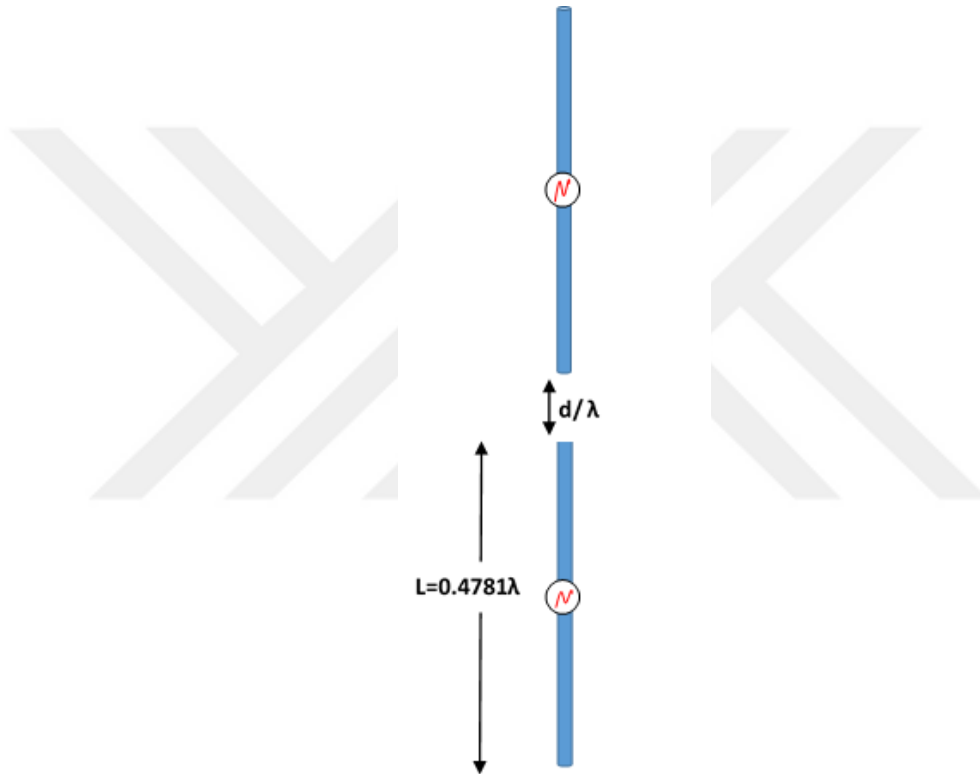
Figure 3.7: Two dipole antennas in collinear arrangement as a function of spacing relative to wavelength with length $L = 0.4781\lambda$ and radius $a = 0.001\lambda$.
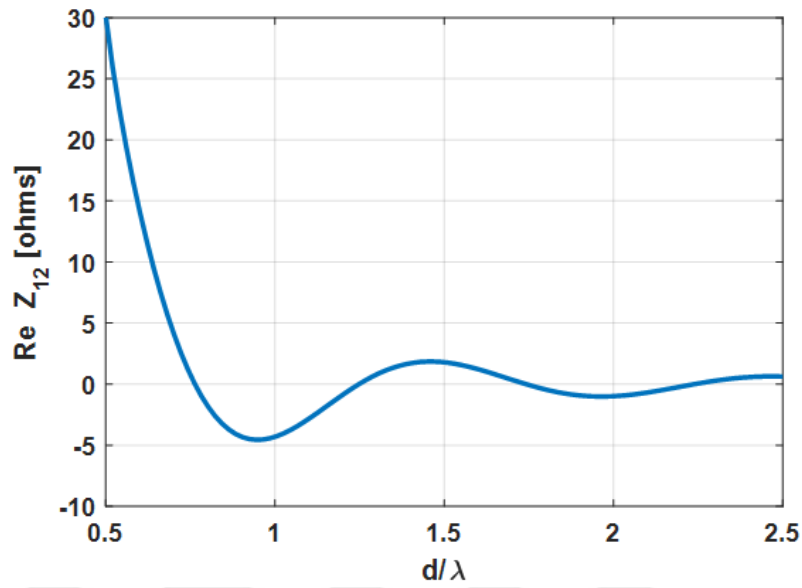
Figure 3.8: Real part of mutual impedance between two collinear dipole antennas as a function of spacing relative to wavelength with length $L = 0.4781\lambda$ and radius $a = 0.001\lambda$.
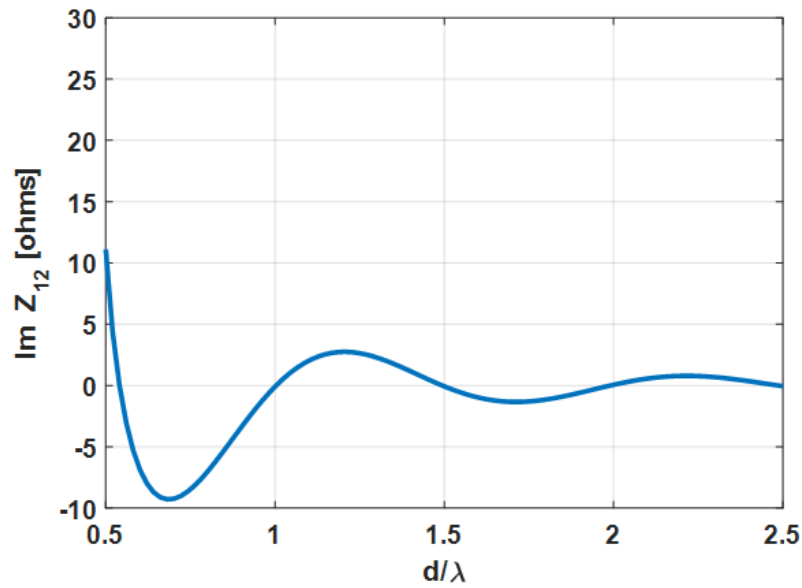
Figure 3.9: Imaginary part of mutual impedance between two collinear dipole antennas as a function of spacing relative to wavelength with length $L = 0.4781\lambda$ and radius $a = 0.001\lambda$.

The results in Fig. 3.8 and 3.9 are in very good agreement with those presented in [2].

3.1.2 Mutual Coupling Compensation

The following subsections present results for the the mutual compensation technique that has been applied to different array configurations shown in the above sections. The uncompensated, compensated, and pattern multiplication patterns are compared. From these patterns it can be observed that the compensation technique explained in section 2.6 works effectively.

#### 3.1.2.1 Two element Uniform Linear Array (ULA)
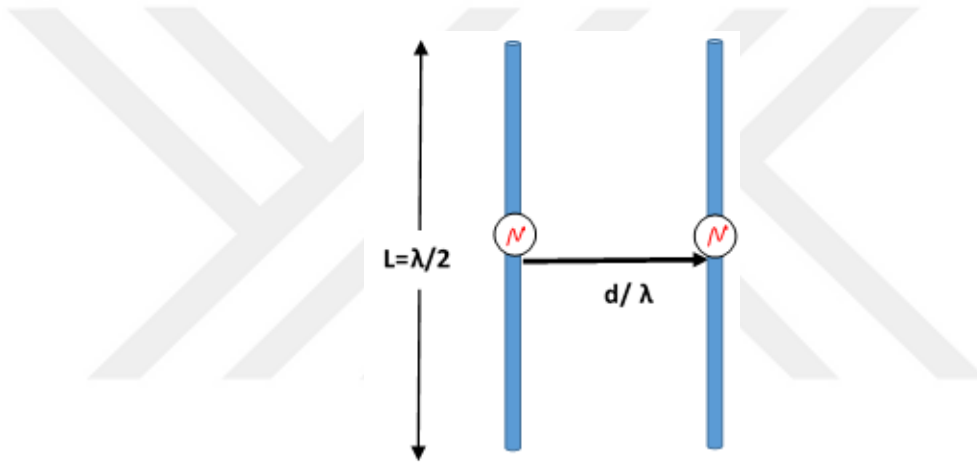
Figure 3.10: Two parallel antennas of length $\lambda/2$ with $a = \lambda/200$.

A two-element dipole antenna array similar to that of [15] with length $\lambda/2$ and radius $\lambda/200$ is used as shown in Fig. 3.10. The antennas are center fed with a magnetic frill source. The antenna element spacing is varied from 0.1λ to 0.5λ. The source internal impedance Z_0 is 50 Ω and the original excitation voltage sources are $V_{g1} = 1\ V$ and $V_{g2} = 1\angle135°V$. The compensated voltages are tabulated in Table 3.1. The results are in close agreement with [15] and [14]. The resultant far field patterns in Figs. 3.11(a-e) show the far field patterns due to the uncompensated voltages, compensated voltages and pattern multiplication method in the plane perpendicular to the dipole axis. It can be observed that the array patterns due to the compensated voltages is almost the same as that of the isolated pattern results computed using pattern multiplication method. When the antennas are spaced closely, there is strong coupling between the antennas. This is evident from Fig. 3.24a as well as the compensated voltages in Table 3.1. The pattern due to the compensated voltage is in close approximation with that of the array factor pattern. As the distance between the dipoles increases the

mutual coupling decreases, therefore, at $d = 0.5\lambda$ the compensated voltages in Table 3.1 become closer to the original voltages.

(a)

(b)

34
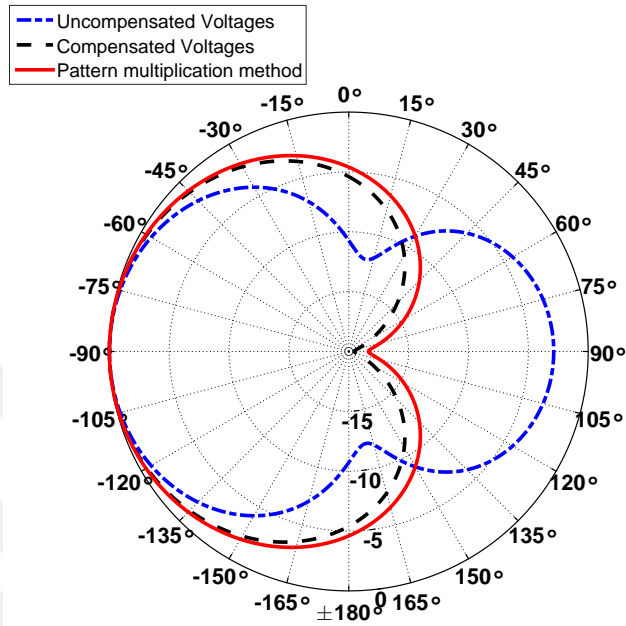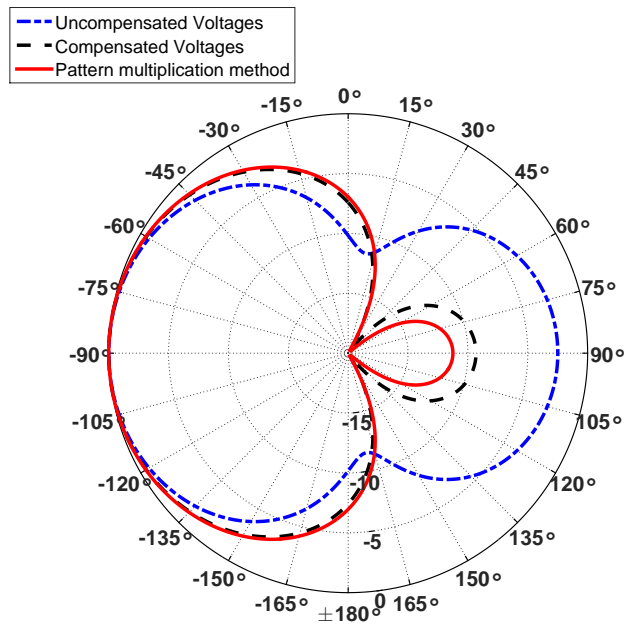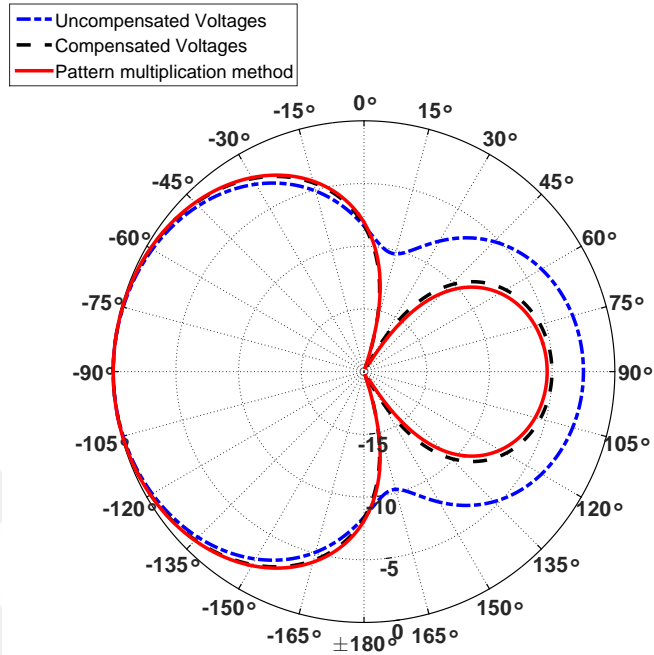
(c)
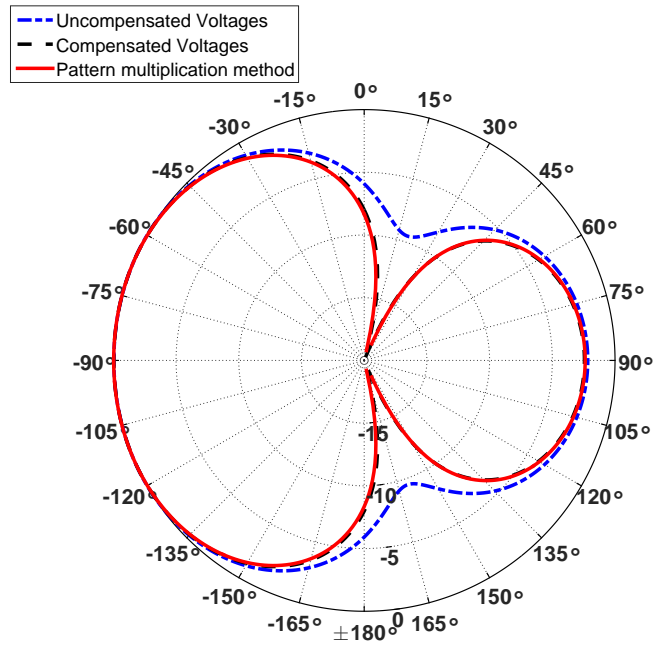
(d)
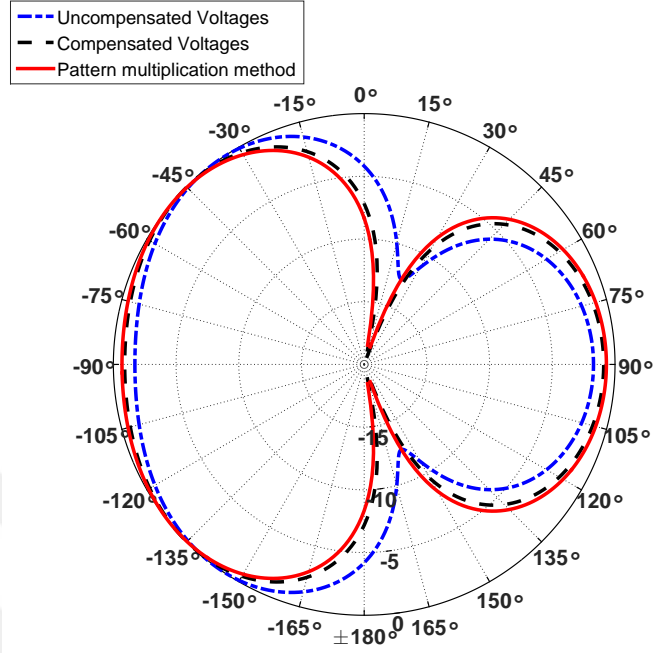
(e)

Figure 3.11: Radiation patterns for two parallel dipole antennas with different element separations. (a) $d = 0.1\lambda$ (b) $d = 0.2\lambda$ (c) $d = 0.3\lambda$ (d) $d = 0.4\lambda$ (e) $d = 0.5\lambda$.

Table 3.1: Compensation voltages V'_{s1} and V'_{s2} for the two element dipole array for different element separations.

Antenna separation $d(\lambda)$	$V'_{s1}, (V)$	$V'_{s2}, (V)$
0.1	$0.870\angle31.58°$	$0.566\angle104°$
0.2	$1.06\angle23.7°$	$0.524\angle134°$
0.3	$1.20\angle15.3°$	$0.692\angle151°$
0.4	$1.27\angle6.81°$	$0.893\angle153°$
0.5	$1.25\angle-1.01°$	$1.05\angle149°$

3.1.2.2 Five Element Uniform Linear Array
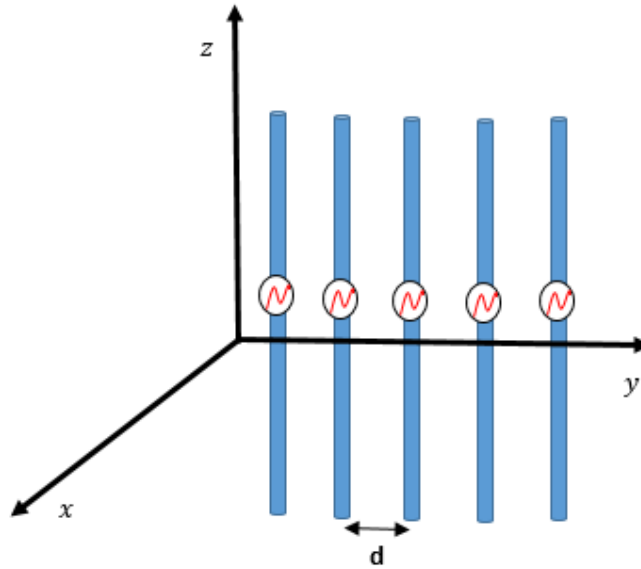
Figure 3.12: Five dipole antennas of length $\lambda/2$, $a = \lambda/200$ and spacing d.

A five element uniform linear array of dipoles as shown in Fig. 3.12 is studied in two different configurations similar to that in [15] and [14]. Same parameters for length, radius and internal source impedances are used as in the case of two-element dipole arrray except for excitation voltages and element spacing. In the first case, $d = 0.5\lambda$ is used as element spacing and main-beam direction is excited at $\varphi = 45°$. The excitation voltages are shown in Table 3.3 [15]. For the second case, $d = 0.3\lambda$ and $\varphi = 60°$. The resultant far field patterns in the plane perpendicular to the dipole axis are shown in Figs. 3.13 and 3.14. The compensated voltages for both cases are tabulated in Table 3.2 which are in close agreement with [15] and [14].
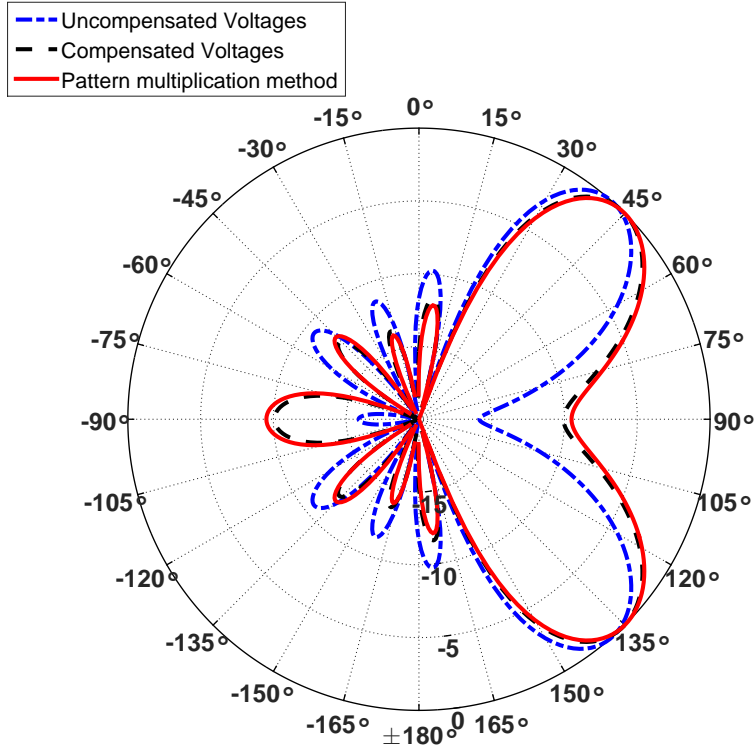
Figure 3.13: Radiation pattern for five-element dipole array with separation $d = 0.5\lambda$ and main-beam direction $\varphi = 45°$.

Table 3.2: Compensation voltages for the five-element dipole array with different inter-element separations d and main-beam directions φ.

| Voltages	$\varphi = 45°,\ d = 0.5\lambda$	$\varphi = 60°,\ d = 0.3\lambda$
V'_{s1}	$0.803\angle 19°$	$0.770\angle -5.34°$
V'_{s2}	$1.12\angle -113°$	$1.19\angle -71.96°$
V'_{s3}	$1.30\angle 110°$	$1.29\angle -127°$
V'_{s4}	$1.37\angle -26.8°$	$1.29\angle 159°$
V'_{s5}	$1.28\angle -168°$	$1.25\angle 116°$
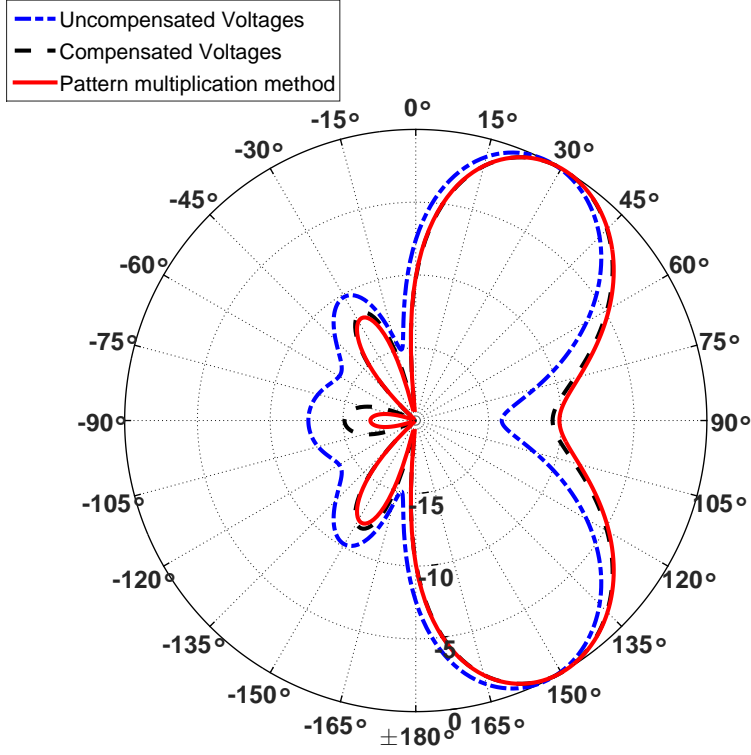
Figure 3.14: Radiation pattern for five-element dipole array with separation $d = 0.3\lambda$ and main-beam direction $\varphi = 60°$.

Table 3.3: Excitation voltages for the five-element dipole array with different inter-element separations d and main-beam directions φ.

Voltages	$\varphi = 45°,\ d = 0.5\lambda$	$\varphi = 60°,\ d = 0.3\lambda$
V_{s1}	$1\angle 0°$	$1\angle 0°$
V_{s2}	$1\angle -127.28°$	$1\angle -54°$
V_{s3}	$1\angle -254.56°$	$1\angle -108°$
V_{s4}	$1\angle -381.84°$	$1\angle -162°$
V_{s5}	$1\angle -509.12°$	$1\angle -216°$

The results infer that when $d = 0.3\lambda$, there is strong mutual coupling which is evident from Table. 3.2 and its corresponding excitation voltages.

3.2   Non-Identical Arrays

3.2.1   Mutual Impedance

The mutual impedance for two element non-identical arrays is calculated in this section. Similar to Section 3.1, three different configurations are studied. Two dipoles of unequal lengths are considered such that $L_1 = \lambda/2$ and $L_2 = \lambda/3$. The radius a for both the wires is same, $a = 0.001\lambda$. The mutual impedance of unequal length dipoles for infinitely thin wires has been studied in [13]. It should be noted that in [13], the author considers infinitely thin wires where as in this thesis a finite wire radius is considered hence the mutual impedances presented in [13] and here are not exactly the same but in close approximation in the overall trend. Figure 3.15 to Fig. 3.20 show the geometry of the arrays considered and the computed mutual impedances.

3.2.1.1   Non Staggered Array
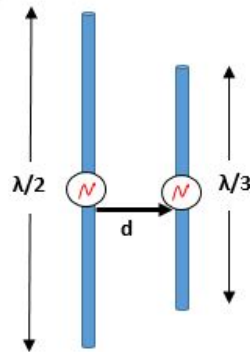
Figure 3.15: Two parallel dipole antennas in non-staggered arrangement of lengths $\lambda/2$ and $\lambda/3$ as a function of spacing relative to wavelength with radius $a = 0.001\lambda$.
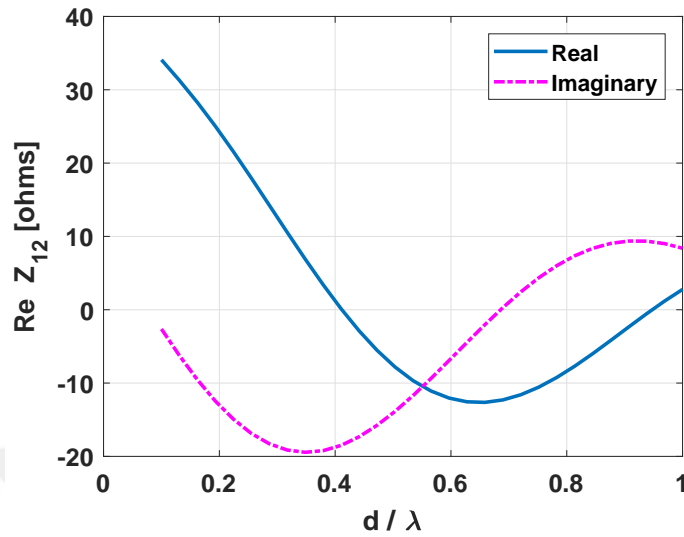
Figure 3.16: Mutual impedance curves between two parallel antennas in non-staggered arrangement of lengths $\lambda/2$ and $\lambda/3$ as a function of spacing relative to wavelength with $a = 0.001\lambda$.

3.2.1.2 Staggered Array
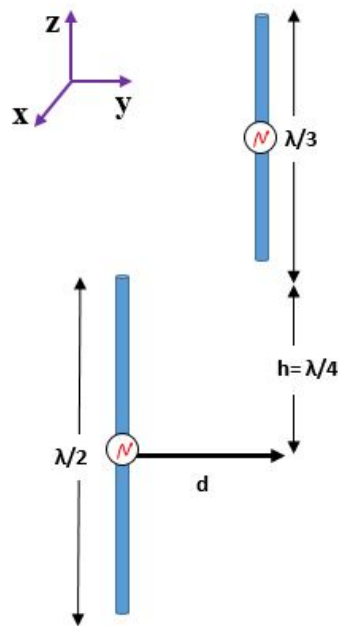
Figure 3.17: Two parallel dipole antennas of lengths $\lambda/2$ and $\lambda/3$ in staggered arrangement as a function of spacing relative to wavelength with $a = 0.001\lambda$, horizontal separation d and staggered by $h = \lambda/4$.
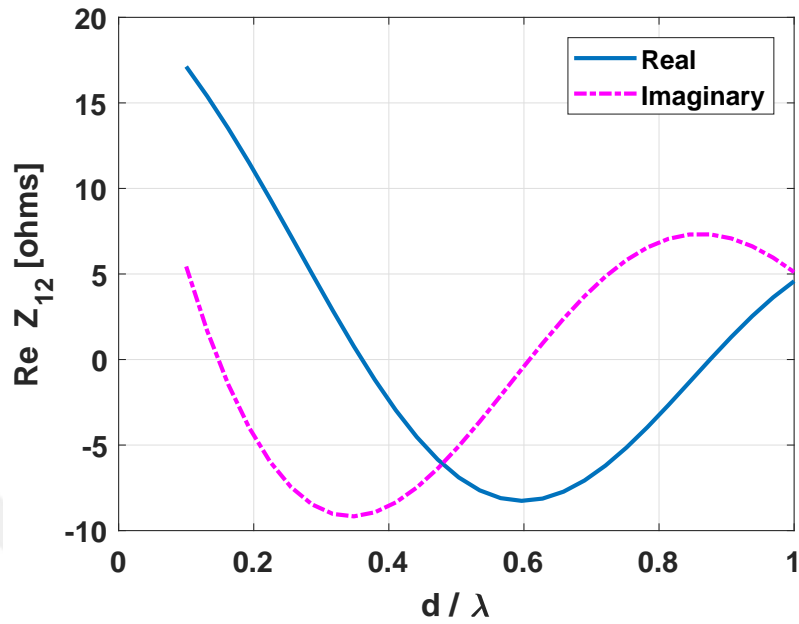
Figure 3.18: Mutual impedance curves between two parallel antennas of lengths $\lambda/2$ and $\lambda/3$ with $a = 0.001\lambda$, staggered by $h = \lambda/4$.

3.2.1.3 Collinear Array
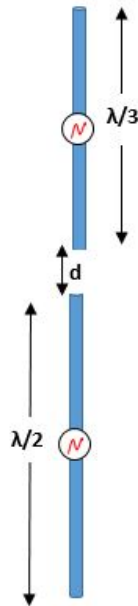
Figure 3.19: Two antennas of lengths $\lambda/2$ and $\lambda/3$ in collinear arrangement as a function of spacing relative to wavelength with radius $a = 0.001\lambda$.
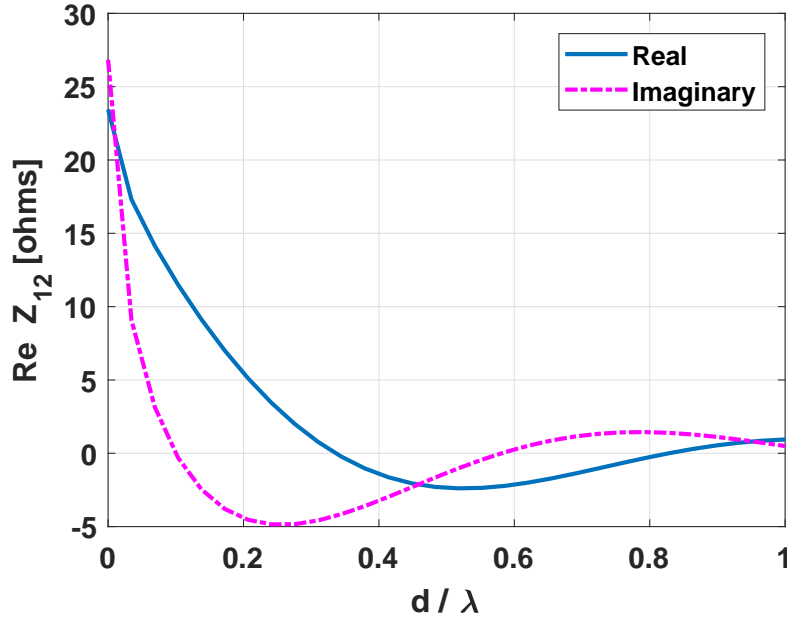
Figure 3.20: Mutual impedance curves for two dipole antennas of lengths $\lambda/2$ and $\lambda/3$ in a collinear arrangement with radius $a = 0.001\lambda$.

3.2.2 Mutual Coupling Compensation

3.2.2.1 Two element Non-Staggered Array

The compensation for two element non-identical array as shown in Fig. 3.21 is computed in this section. The dipoles are excited with a magnetic frill source at their center. The original excitation voltage sources are $V_{g1} = 1\ V$ and $V_{g2} = 1\angle 135°V$, respectively. The antenna element spacing is varied from 0.1λ to 0.5λ. The compensated voltages are tabulated in Table 3.4. The resultant far field patterns in Figs. 3.22(a-e) show the far field patterns due to the uncompensated voltages, compensated voltages and pattern multiplication method in the plane perpendicular to the dipole axis, i.e., the H-plane. As compared to the identical two element dipole case in Fig. 3.11 and Table 3.1, it can be noted that the mutual coupling is weaker here since L_2 is shorter than L_1 we expect less coupling.
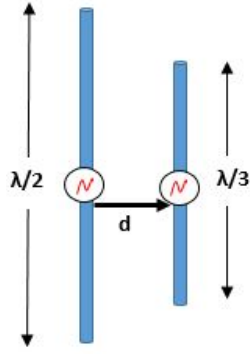
Figure 3.21: Two parallel antennas in non-staggered arrangement of lengths $\lambda/2$ and $\lambda/3$ as a function of spacing relative to wavelength with radius $a = 0.001\lambda$, and separation d.

**Table 3.4:** Compensation voltages V'_{s1} and V'_{s2} of two-element non-identical non-staggered dipole array for different antenna separations.

Antenna separation $d(\lambda)$	$V'_{s1}, (V)$	$V'_{s2}, (V)$
0.1	$0.8199\angle-6.46°$	$0.7517\angle128.0°$
0.2	$0.8307\angle-0.65°$	$0.7723\angle135.2°$
0.3	$0.8752\angle3.56°$	$0.8314\angle140.7°$
0.4	$0.9360\angle5.29°$	$0.9117\angle142.9°$
0.5	$0.9921\angle4.92°$	$0.9877\angle142.3°$
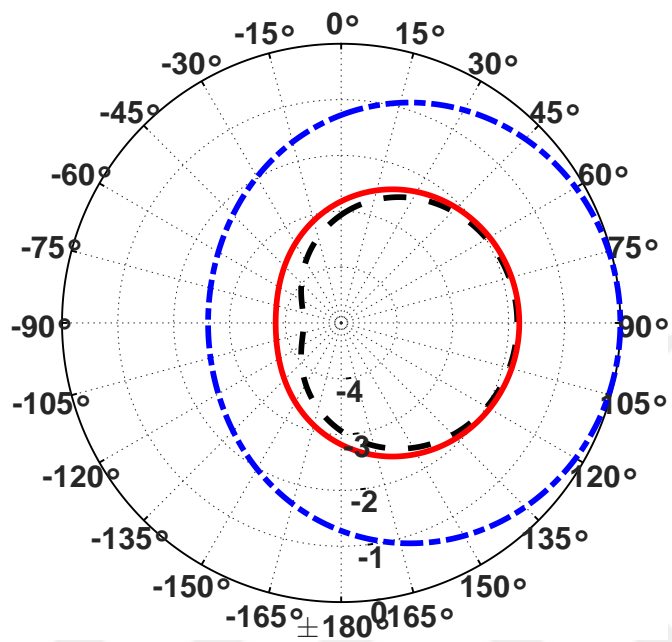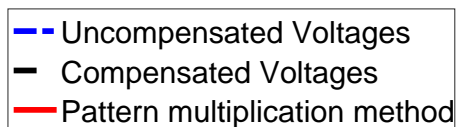
(a)
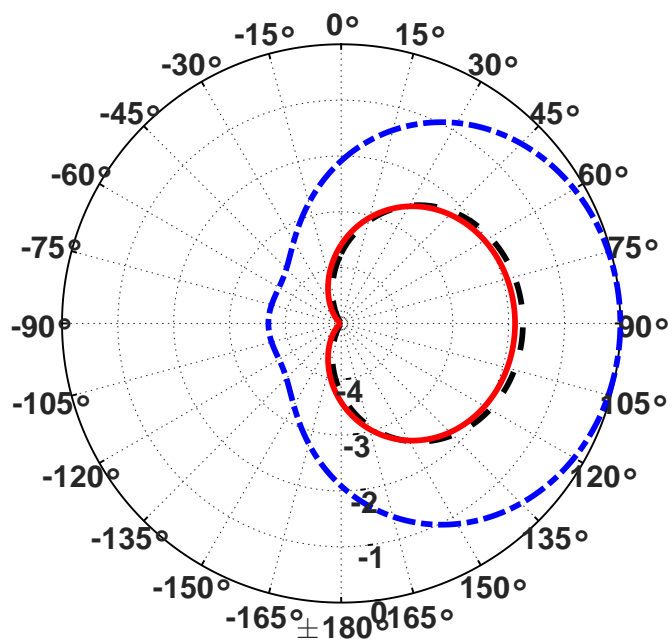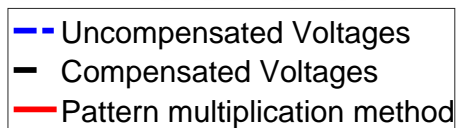
(b)

45

(c)

(d)

46
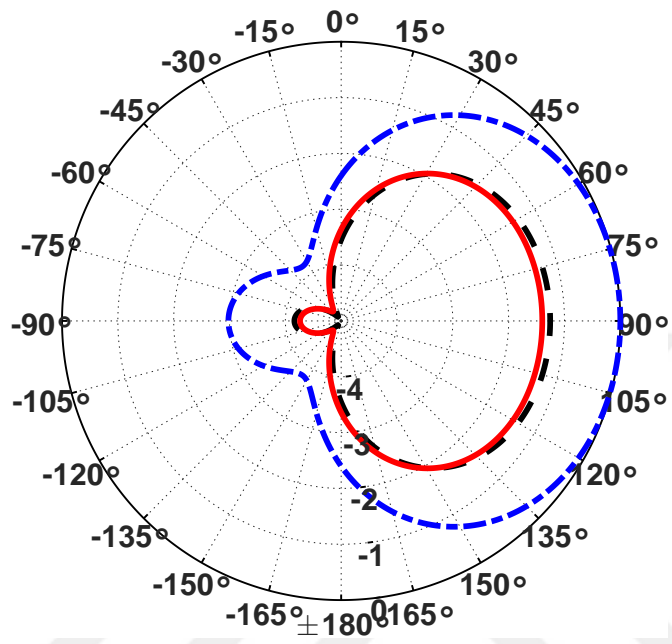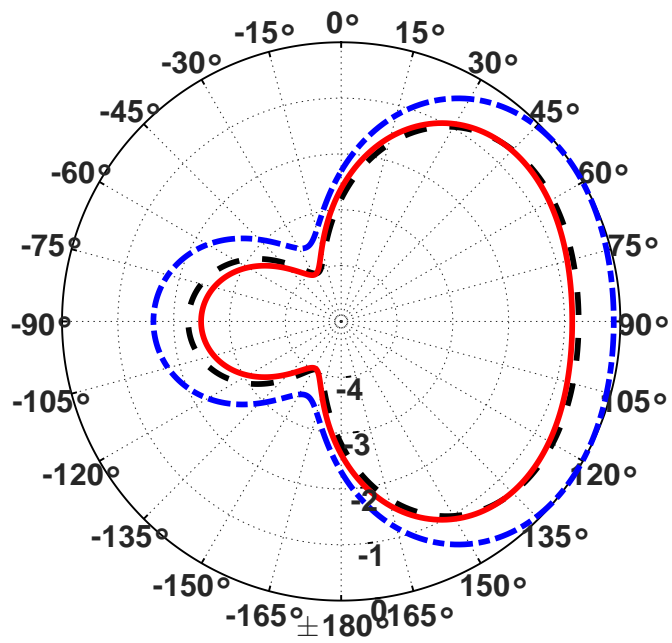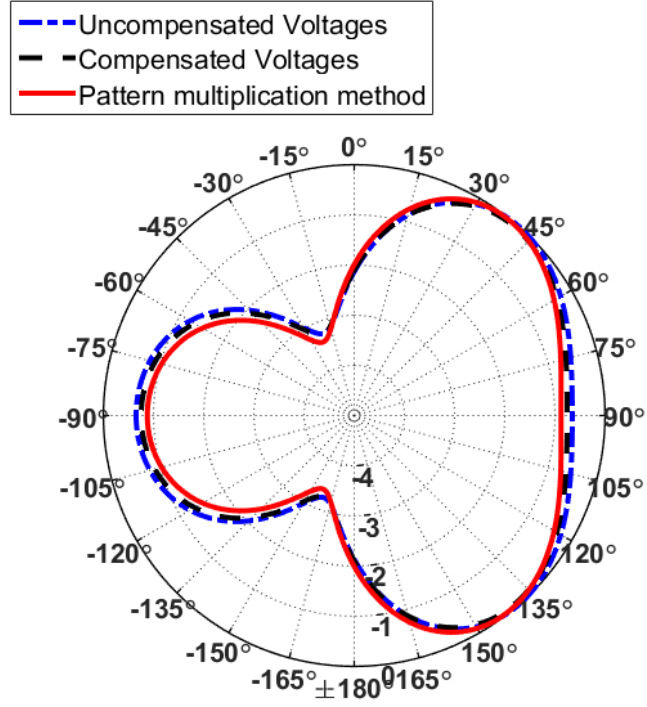
(e)

Figure 3.22: Radiation pattern of two-elements non-identical non-staggered dipoles with different element separations. (a) $d = 0.1\lambda$ (b) $d = 0.2\lambda$ (c) $d = 0.3\lambda$ (d) $d = 0.4\lambda$ (e) $d = 0.5\lambda$.

3.2.2.2 Two Elements Staggered Array

The compensation for two elements non-identical staggered array as shown in Fig. 3.23 is computed in this section. The dipoles are staggered by $h = \lambda/4$. With excitation source voltages $V_{g1} = 1\ V$ and $V_{g2} = 1\angle135°V$ and element spacing varied from 0.1λ to 0.5λ, the compensated voltages are tabulated in Table 3.5. The resultant far field patterns in Figs. 3.24(a-e) show the far field patterns due to the uncompensated voltages, compensated voltages and pattern multiplication method in the plane perpendicular to the dipole axis. As compared to the identical two element dipole case in Fig. 3.11 and Table 3.1, it can be noted that the mutual coupling is weaker here since L_2 is not in line with L_1, which results in weak coupling.

47
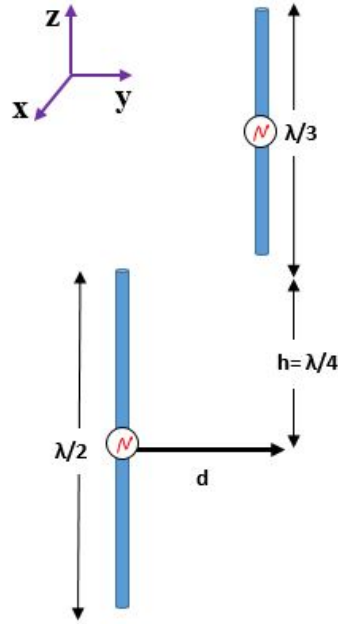
Figure 3.23: Two parallel dipole antennas of lengths $\lambda/2$ and $\lambda/3$ in staggered arrangement as a function of spacing relative to wavelength with radius $a = 0.001\lambda$, and staggered by $h = \lambda/4$.

Table 3.5: Compensation voltages V'_{s1} and V'_{s2} for two-elements non-identical staggered dipole array for different antenna separations.

| Antenna separation $d(\lambda)$	$V'_{s1}, (V)$	$V'_{s2}, (V)$
0.1	$0.9278\angle-4.83°$	$0.8893\angle129.1°$
0.2	$0.9230\angle-0.81°$	$0.8902\angle134.5°$
0.3	$0.9453\angle1.71°$	$0.9221\angle137.9°$
0.4	$0.9782\angle2.62°$	$0.9670\angle139.1°$
0.5	$1.0081\angle2.27°$	$1.0082\angle138.5°$

(a)

(b)

(c)
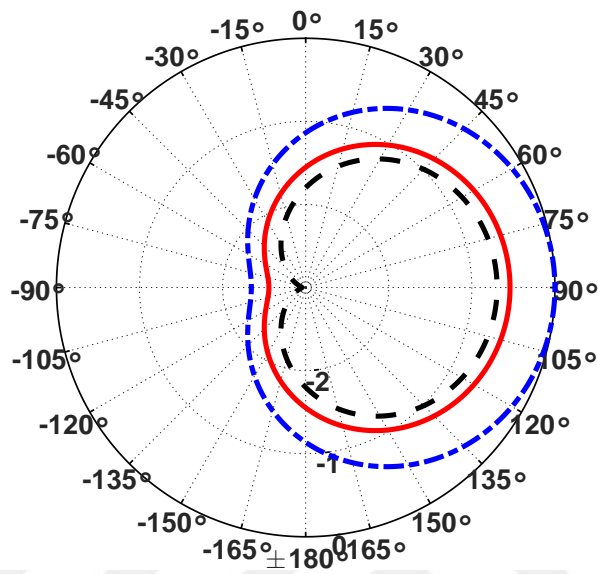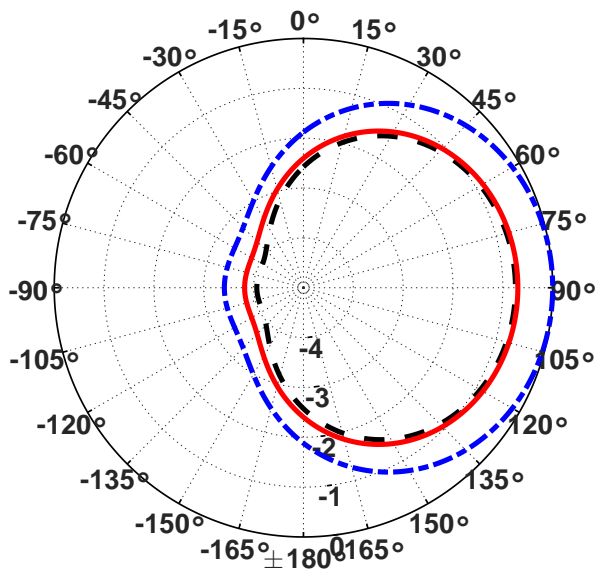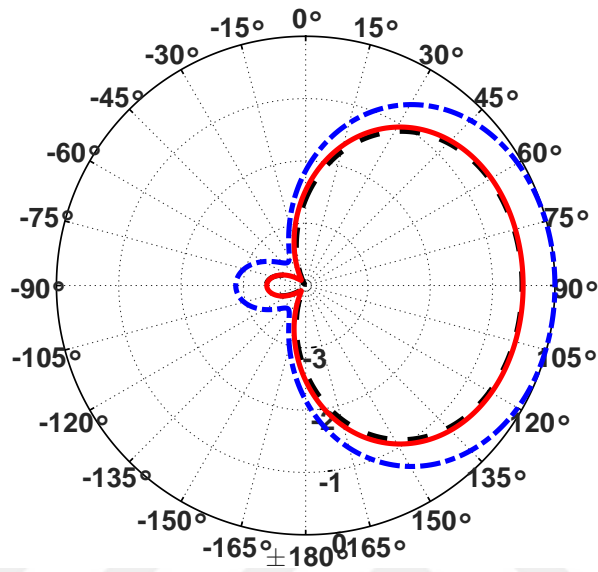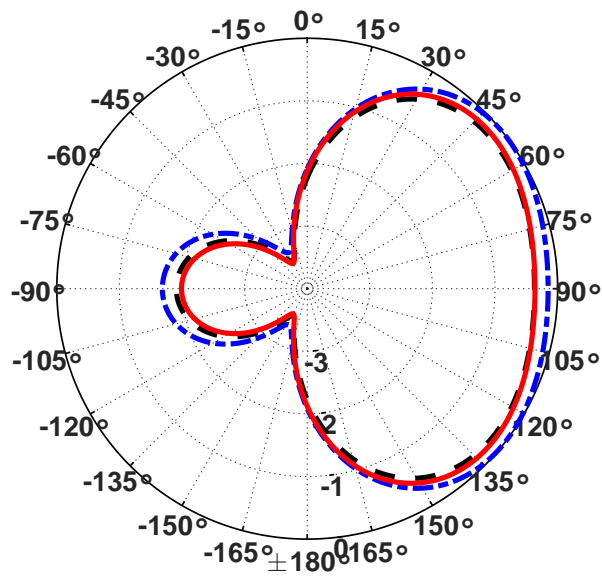
(d)
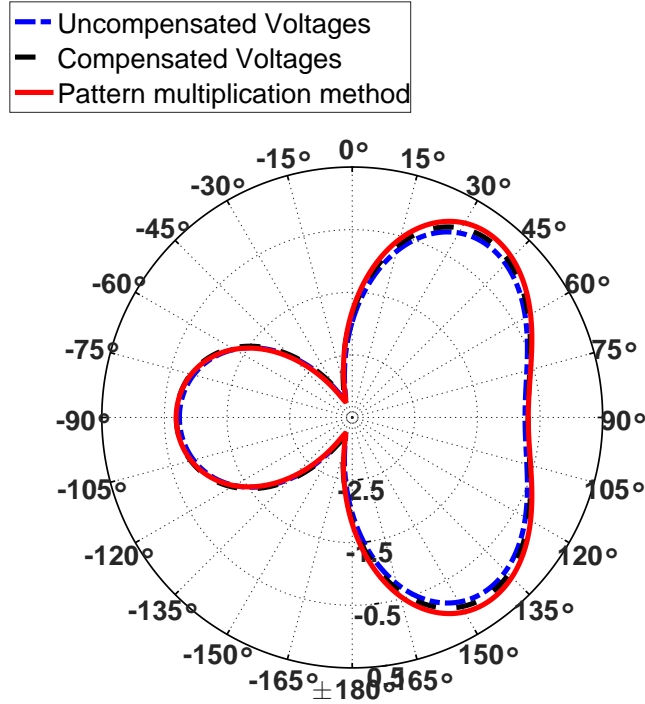
(e)

Figure 3.24: Radiation pattern of two-element non-identical staggered dipoles with different element separations. (a) $d = 0.1\lambda$ (b) $d = 0.2\lambda$ (c) $d = 0.3\lambda$ (d) $d = 0.4\lambda$ (e) $d = 0.5\lambda$.

3.2.2.3   Two element Collinear Array

When the dipoles are in a collinear arrangement as shown in Fig. 3.25. With the excitation voltage sources $V_{g1} = 1\ V$ and $V_{g2} = 1\angle135°V$ and element spacing varied from 0.1λ to 0.5λ, it can be observed from Table 3.6 that the mutual coupling is extremely weak. The values are approximately equal to the original excitation values which infers to the weak coupling. This is also evident from the mutual impedance shown in Fig. 3.20. In this case the three patterns are almost identical and therefore not plotted here.
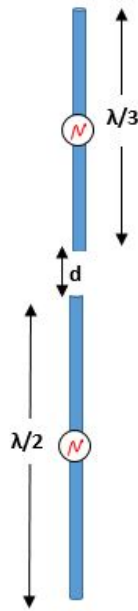
Figure 3.25: Two antennas of lengths $\lambda/2$ and $\lambda/3$ in collinear arrangement as a function of spacing relative to wavelength with $a = 0.001\lambda$.

**Table 3.6:** Compensation voltages V'_{s1} and V'_{s2} of two-element non-identical collinear dipole array for different antenna separations.

Antenna separation $d(\lambda)$	$V'_{s1}, (V)$	$V'_{s2}, (V)$
0.1	$0.9339\angle-2.2°$	$0.9018\angle132.7°$
0.2	$0.9502\angle0.19°$	$0.9274\angle135.9°$
0.3	$0.9707\angle0.97°$	$0.9558\angle136.8°$
0.4	$0.9869\angle0.93°$	$0.9777\angle136.7°$
0.5	$0.9965\angle0.56°$	$0.9905\angle136.2°$

3.2.2.4   Three element Staggered Array

This section presents three dipole elements with lengths $L_1 = \lambda/2$, $L_2 = \lambda/4$ and $L_3 = \lambda/3$. The dipoles are uniformly excited with $V = 1\ V$ and have similar radii $a = 0.001\lambda$. The three wires are arranged as shown in Fig. 3.26.
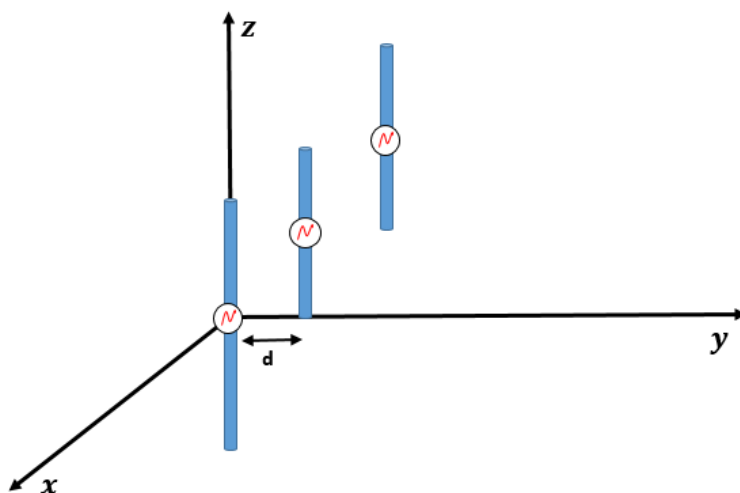
Figure 3.26: Three staggered dipole antennas of different lengths $L_1 = \lambda/2$, $L_2 = \lambda/4$, $L_3 = \lambda/3$.

The elements are equally spaced with $d = 0.1\lambda$ along y-axis. The center of the first dipole is at origin where as the other two dipoles are staggered along z-axis. The far-field radiation patterns in the three principle planes are shown below,
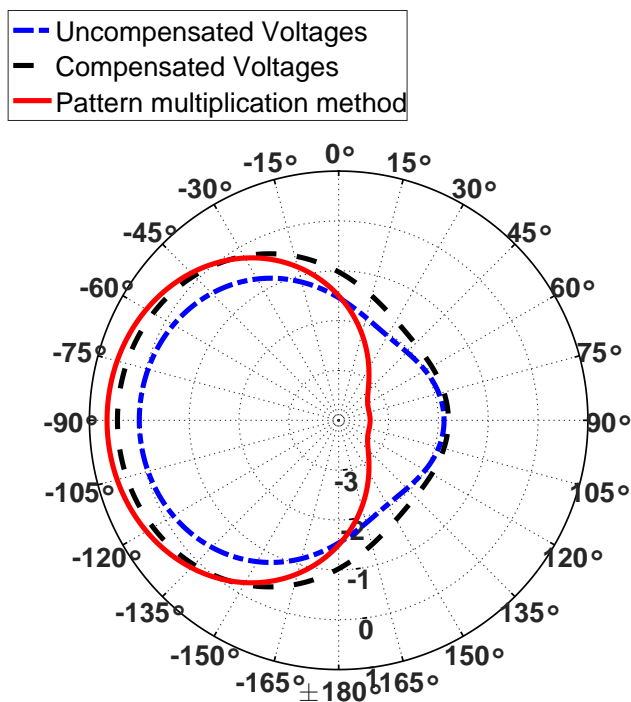
Figure 3.27: Radiation pattern of three element staggered array in xy-plane at 300 MHz.

53
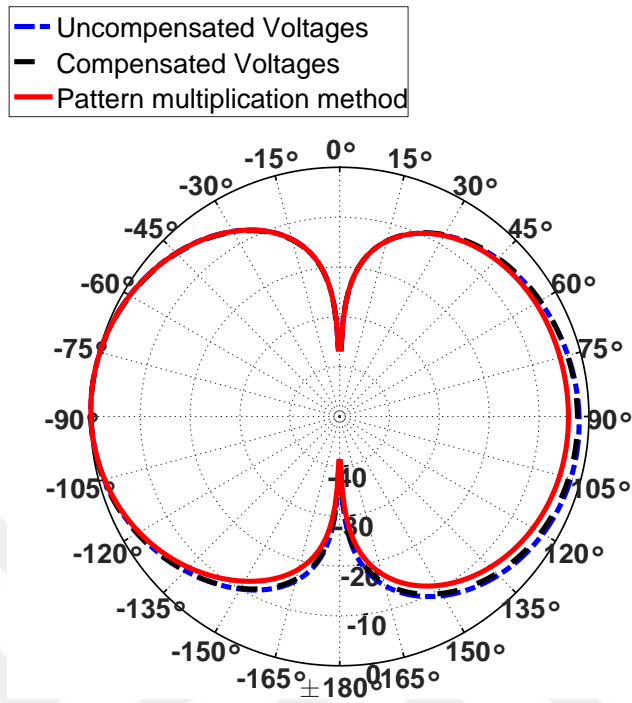
Figure 3.28: Radiation pattern of three element staggered array in yz-plane at 300 MHz.
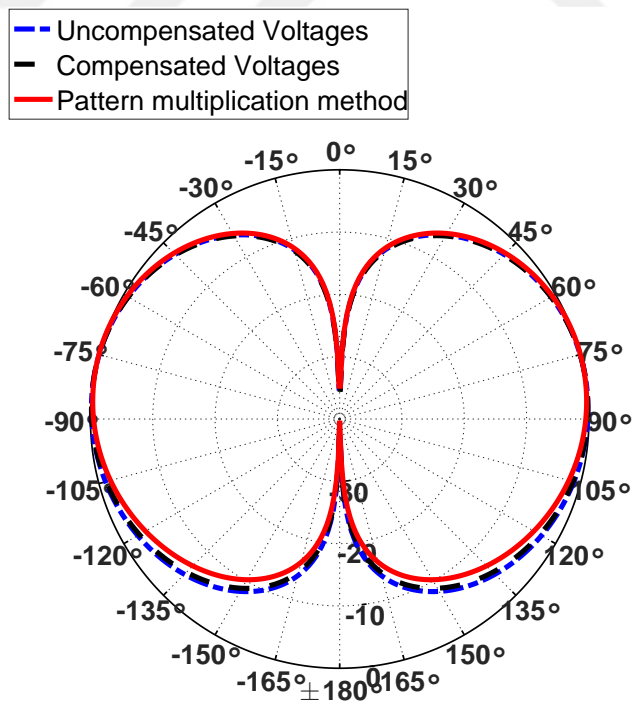
Figure 3.29: Radiation pattern of three element staggered array in xz-plane at 300 MHz.

3.3 Compensation of Circular Arrays

The compensation for dipoles arranged in a circular array has been studied and presented in this section. Identical dipoles have been used in two different cases. In the first case, four dipole elements are arranged in a circle. Since there are only four antennas this means the antennas will be placed at $\varphi = 0°, 90°, 180°$, and $360°$. When viewed from the top the arrangement appears to be similar to a square array. In the second case, three dipole elements are arranged in a circle with equal angles apart similar to a triangle.

3.3.1 Square Array

Four dipole elements arranged around a circle with equal angles apart is shown in Fig. 3.30. The radius of the circle is $\lambda/4$. All elements are uniformly excited with $V = 1V$ where as the elements have $L = 0.5\lambda$, $a = 0.001\lambda$ and $N = 9$.

<div align="center">(a)   (b)</div>
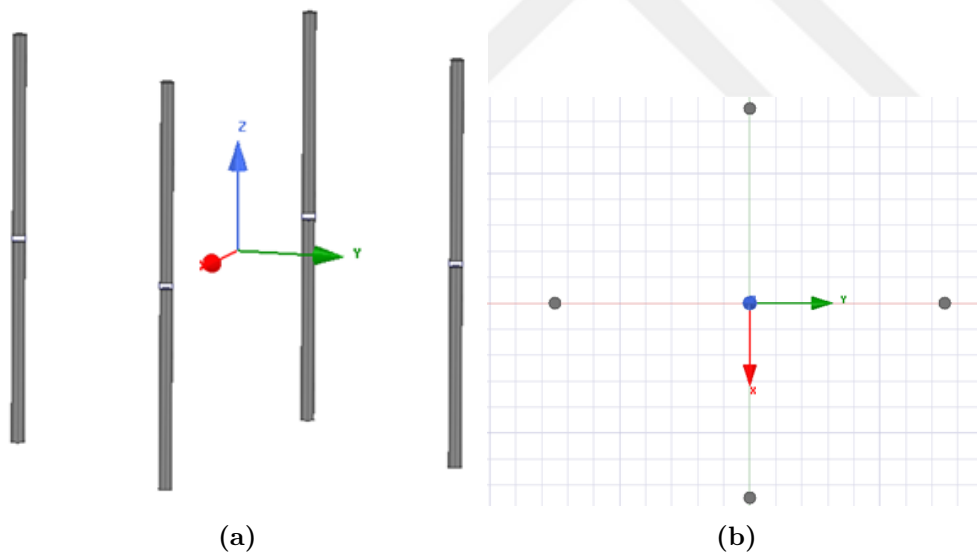
Figure 3.30: Circular array of four half-wave dipoles with radius of circle $\lambda/4$. a) Side view. b) Top view.

Figure 3.31 shows the far-field pattern of the square array, in the plane perpendicular to the axis of the dipoles, when all elements are uniformly excited with $1V$. Since the excitation is same and all elements are identical we expect that the effect of every element on the other is balanced due to symmetry and hence mutual coupling is automatically compensated.

Here we can see that the three curves are identical and that the original patterns i.e (uncompensated patterns) are the same as the array factor. Note that all patterns computed in this work are normalized.
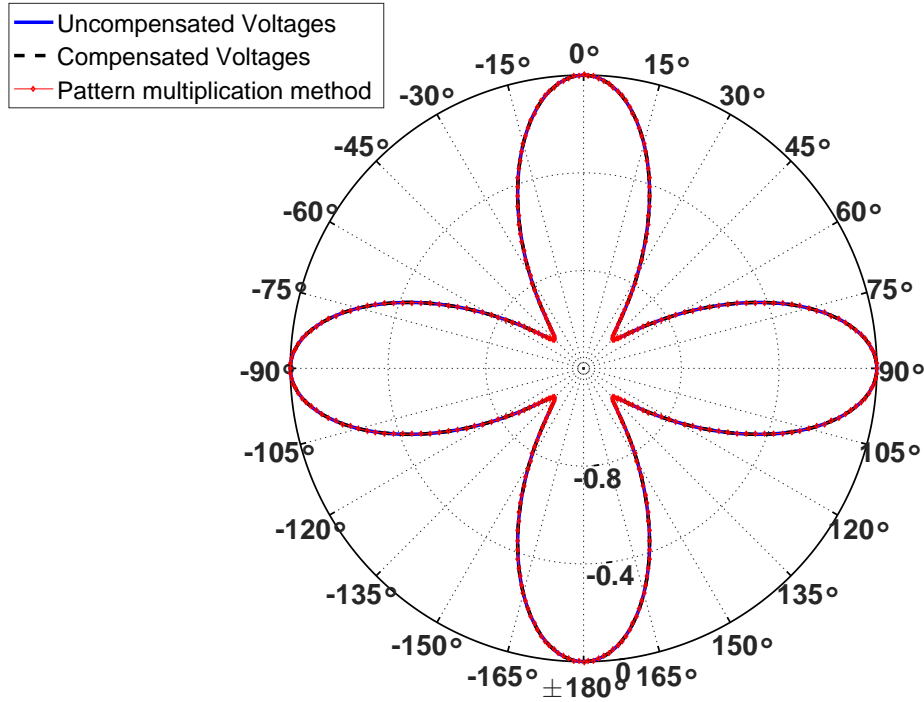
Figure 3.31: Radiation pattern of four element circular array in XY plane at 300 MHz with uniform excitation.

The current distribution is shown in Fig. 3.32 below. The current distribution is symmetric on the four antennas. The original uncompensated currents are observed when the four antennas are uniformly excited with $V = 1\,V$. The compensated currents are computed when the four antennas are excited by $V' = 0.19\angle 58°$. The isolated currents are that of a single antenna when it is excited by $V = 1\,V$ in isolation. Since the *distribution* of these three currents are identical the *normalized* pattern produced by them will be identical as shown in Fig. 3.31.
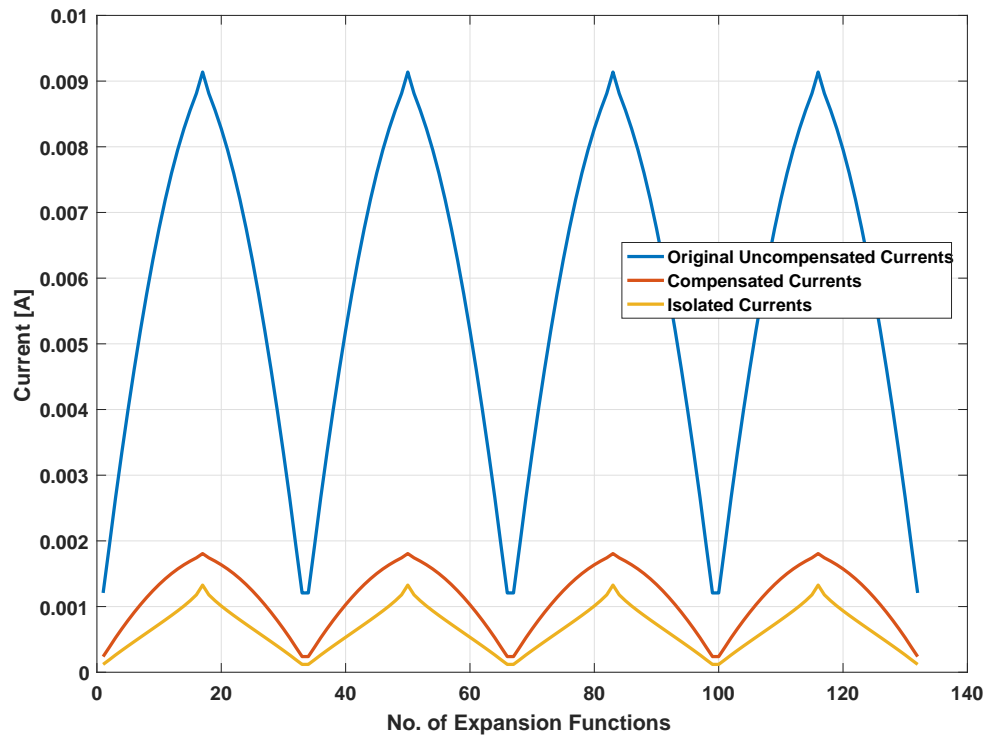
Figure 3.32: Current distribution of the four dipole array when all antennas are uniformly excited.

Now when the excitation is changed to progressive phase excitation with $V_1 = 1\angle 0°$, $V_2 = 1\angle 30°$, $V_3 = 1\angle 60°$ and $V_4 = 1\angle 90°$, it can be observed that coupling between the elements causes different patterns as shown in Fig. 3.33 below.
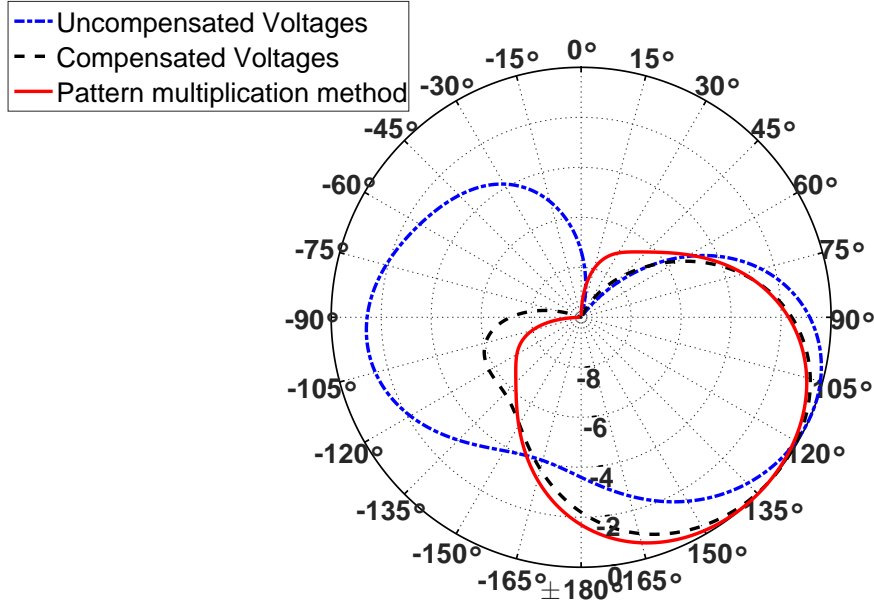
Figure 3.33: Radiation pattern of four element circular array in XY plane at 300 MHz with progressive phase excitation.

Figure 3.33 is the main motivation behind this thesis. The pattern multiplication method can predict the far-field pattern of identical arrays but without mutual coupling. We expect the radiated pattern to be the same as the one predicted by the pattern multiplication method but due to mutual coupling we get a completely different pattern. This phenomenon is illustrated distinctively in Fig. 3.33. The pattern after compensation is in close agreement to that of the pattern multiplication which is a manifestation of how simple and easy a technique can be applied to compensate for thin wire antennas. The current *distribution* is shown in Fig. 3.34. It can be seen that the currents are not symmetric because of the progressive phase excitation. The original uncompensated currents are observed when the four antennas are excited with $V_1 = 1\angle 0°$, $V_2 = 1\angle 30°$, $V_3 = 1\angle 60°$ and $V_4 = 1\angle 90°$. The compensated currents are computed when the four antennas are excited with $V_1' = 0.29\angle 83°$, $V_2' = 0.23\angle 94°$, $V_3' = 0.16\angle 136°$ and $V_4' = 0.056\angle 177°$. The isolated currents are that of a single antenna when it is excited by $V = 1\ V$ in isolation similar to that in Fig. 3.32.
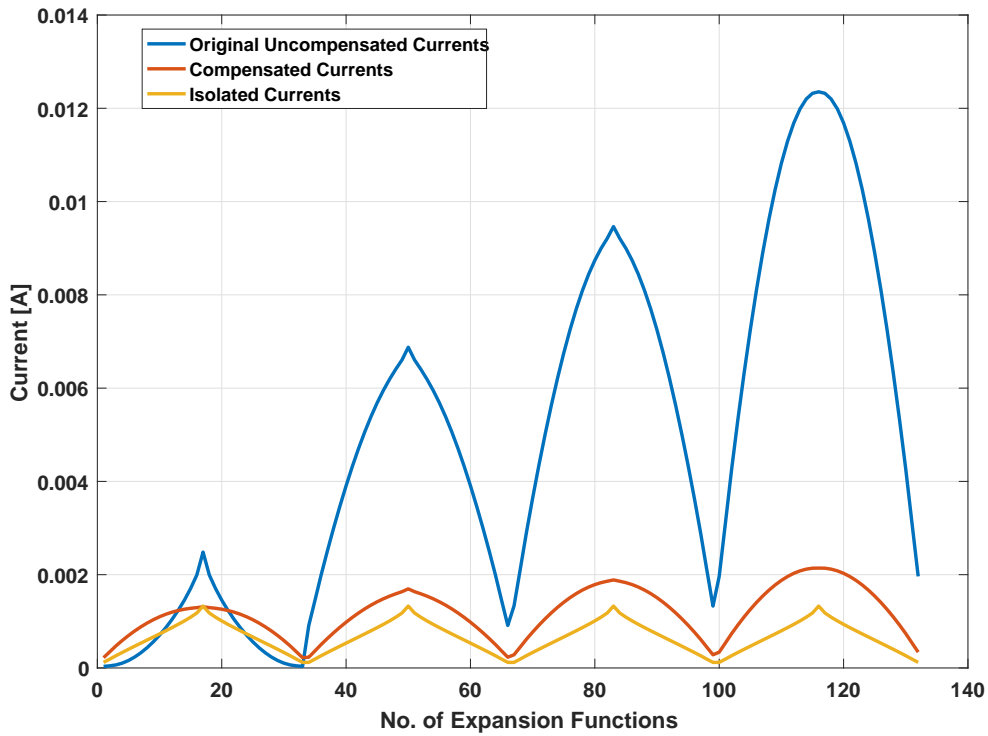
Figure 3.34: Current distribution of the four dipole array when antennas are excited with a progressive phase.

3.3.2 Triangular Array

This section presents three dipoles arranged in a circle to form a triangular array. The same configuration has been used as that of the square array except that now only three elements are used. The setup can be seen in Fig. 3.35.
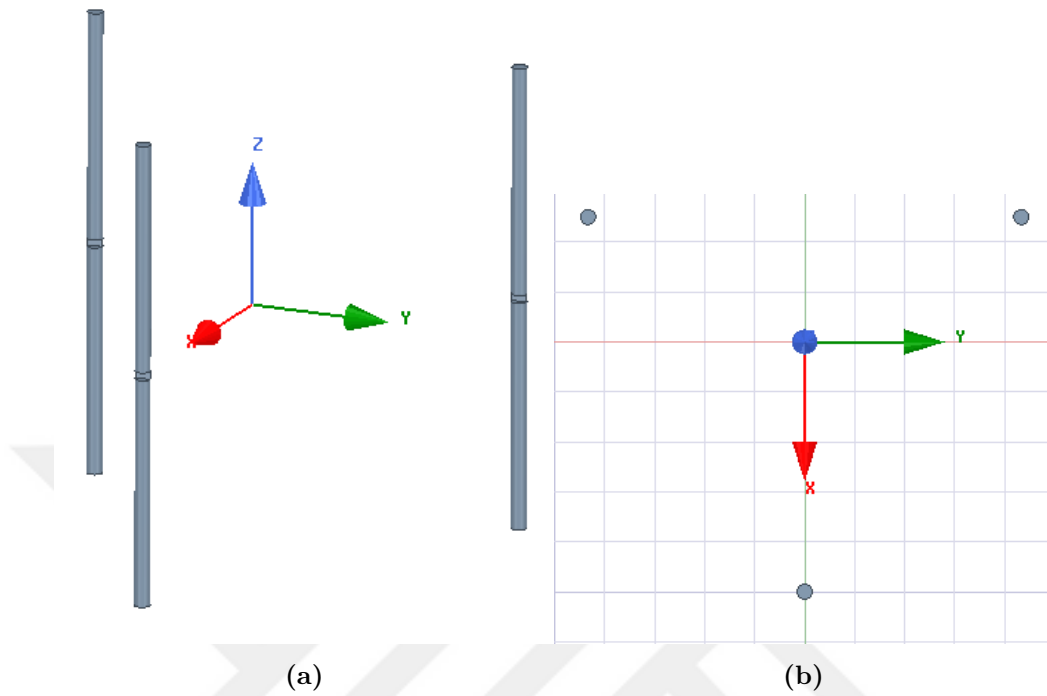
Figure 3.35: Triangular array of three dipole antennas. a) Side view. b) Top view.

When the array is uniformly excited it is observed that mutual coupling effect is not apparent as it has been compensated due to symmetry and can be seen in the far-field pattern shown in Fig. 3.36.
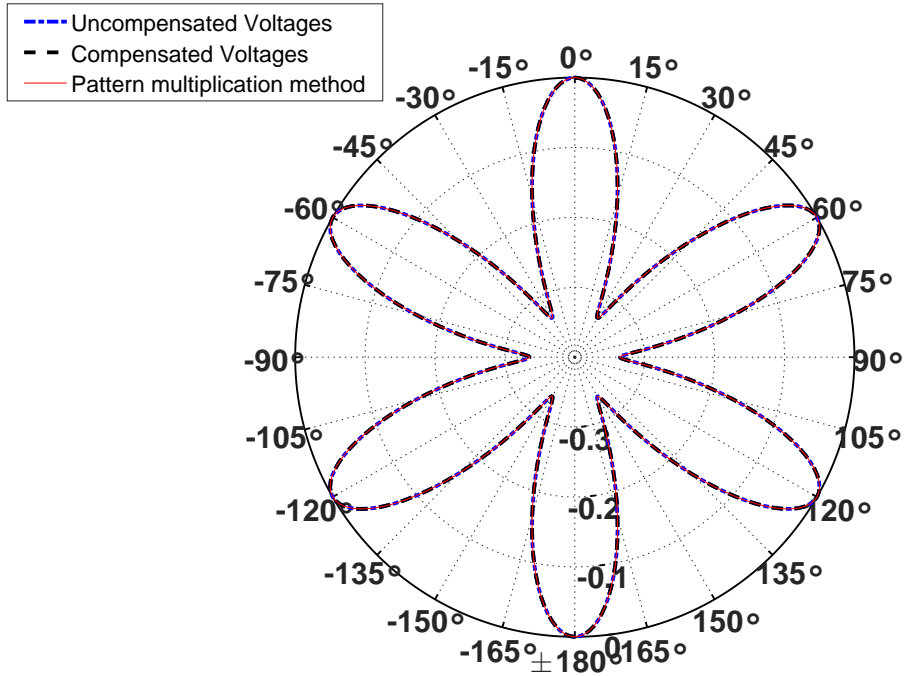
Figure 3.36: Radiation pattern of three element triangular array in xy-plane at 300 MHz with uniform excitation.

When the array is excited with phase progression with $V_1 = 1\angle 0°$, $V_2 = 1\angle 30°$ and $V_3 = 1\angle 60°$ mutual coupling effect shows itself as shown in the three patterns of Fig. 3.37.
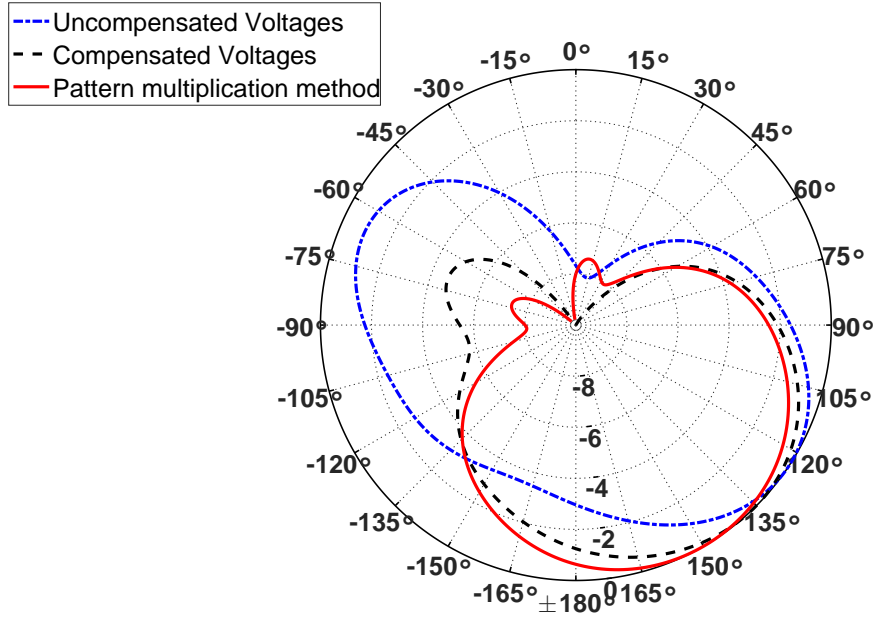
Figure 3.37: Radiation pattern of three element triangular array in XY plane at 300MHz with progressive phase excitation.

Once again the compensation for mutual coupling can be seen evidently which conforms the success of this method.

3.4 Compensation of 3-Dimensional Circular Arrays

In the previous sections, compensation for planar arrays was discussed. Now, 3-dimensional (3D) arrays are studied as shown in Fig. 3.38. Seven dipoles are arranged in two circles. Four dipoles are place along a circle in the lower ring and three dipoles in the upper circular ring i.e., displaced along z-axis.
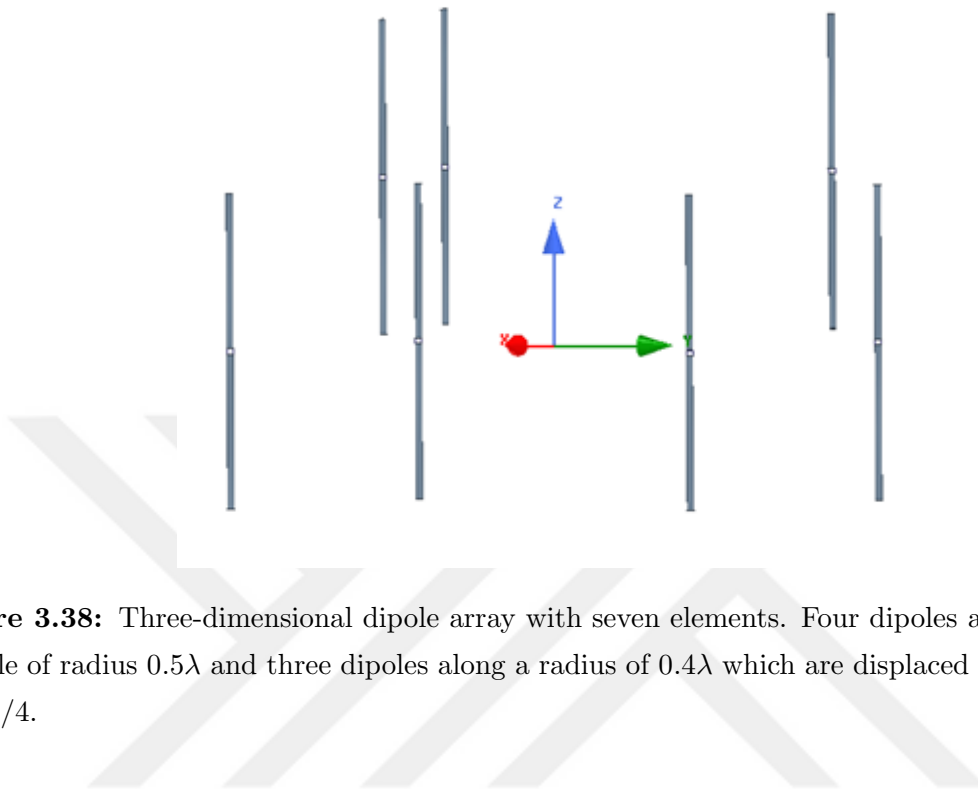
Figure 3.38: Three-dimensional dipole array with seven elements. Four dipoles are placed along a circle of radius 0.5λ and three dipoles along a radius of 0.4λ which are displaced in the z-axis by $h = \lambda/4$.

The dipoles are identical having length $L = \lambda/2$ and radius $a = \lambda/500$. The lower circular ring has a radius of 0.5λ and the upper has a radius of 0.4λ. The center of the dipoles in the lower ring are at $z = 0$ plane where as the center of the upper dipoles are at $z = \lambda/4$ plane. All elements are uniformly excited and the far-field patterns in the three principle planes are shown in Figs. 3.39 to 3.41.
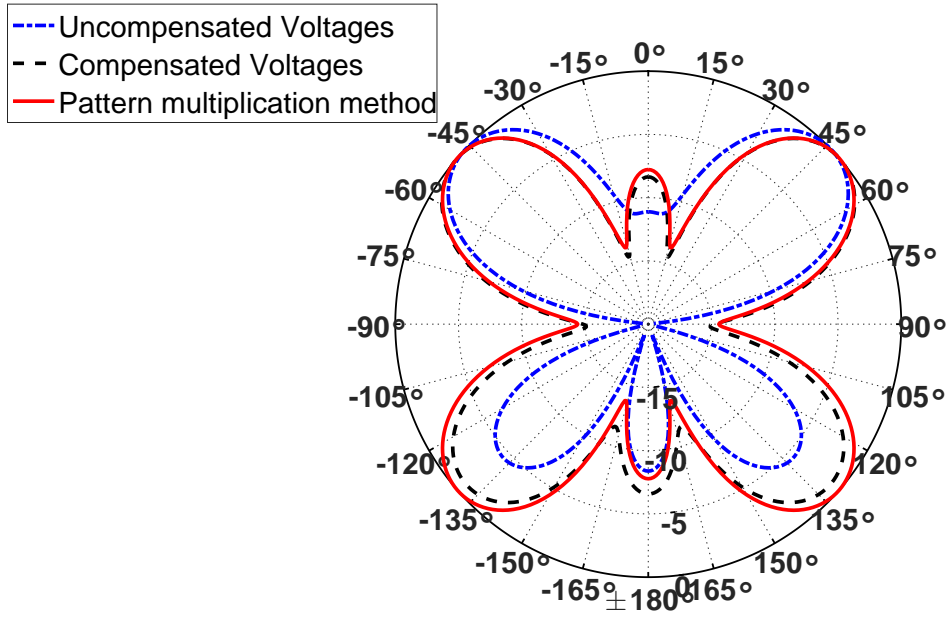
Figure 3.39: Radiation pattern in xy-plane for a 3-Dimensional dipole array at 300 MHz.
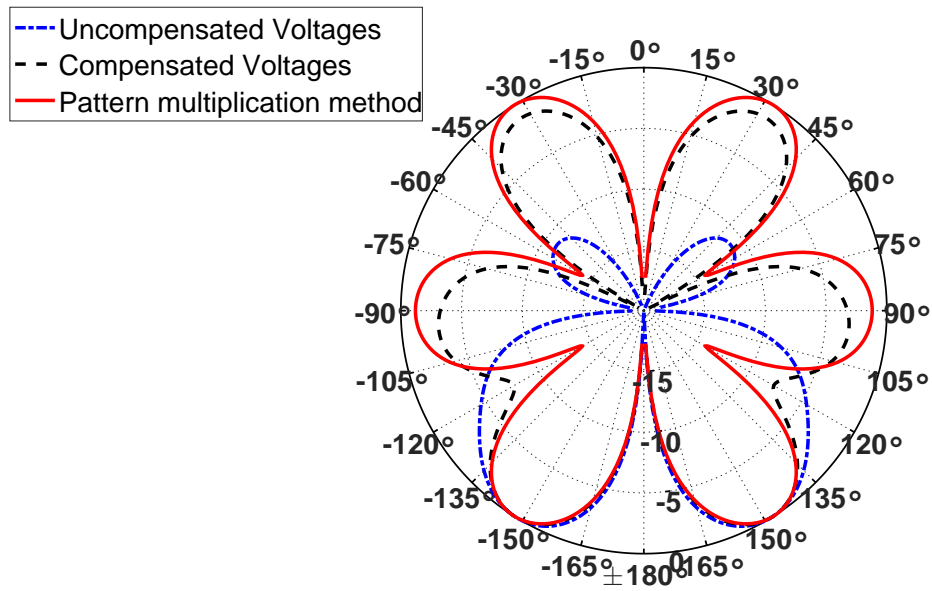
Figure 3.40: Radiation pattern in yz-plane for a 3-Dimensional dipole array at 300 MHz.
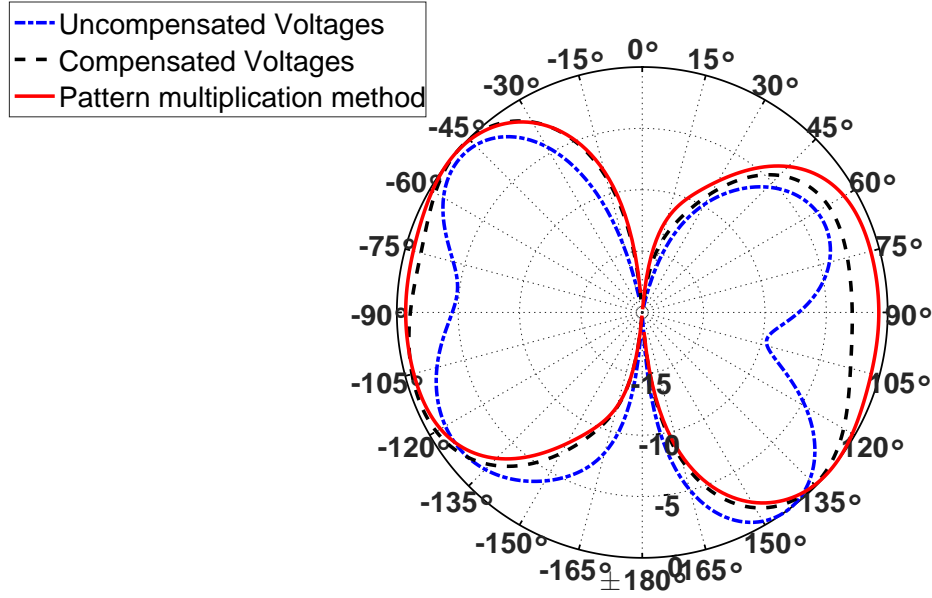
Figure 3.41: Radiation pattern in xz-plane for a 3-Dimensional dipole array at 300 MHz.

3.5 Comparison with commercial software

All the results shown in this thesis are simulated using MATLAB. In order to verify the computed results with commercial software, HFSS was used. In this section the far-field patterns for the three-dimensional array and square array are compared. In the 3D case the setup is similar to Fig. 3.38. The dipole was first resonated at 1 GHz and then used in an array setup as shown in Fig. 3.38. The array was uniformly excited with 1 V using lumped ports with 50 Ω port impedance. The simulation was run with a medium mesh size. In order to resonate the dipole the length was shortened to 0.45λ and radius $a = 3/400\lambda$ was used. The far-field patterns with mutual coupling from HFSS are plotted and compared with those obtained from MATLAB as shown in Figs. 3.42 to 3.44.
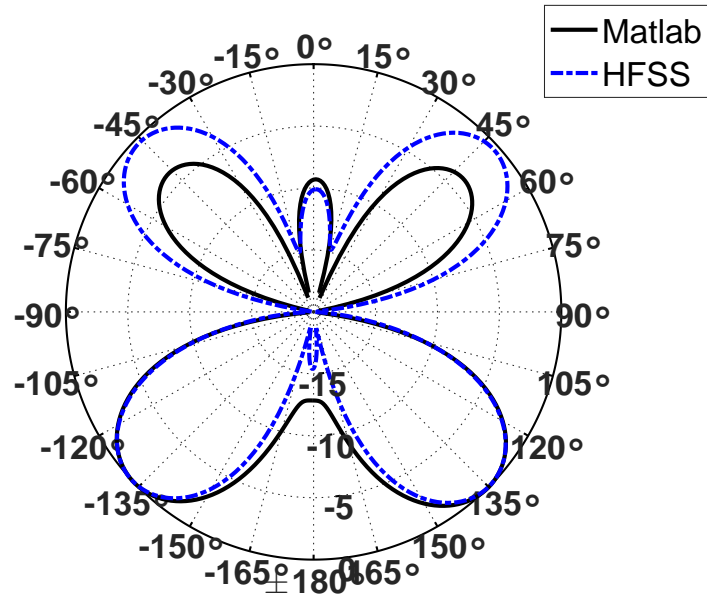
Figure 3.42: Radiation pattern comparison of HFSS and MATLAB in xy-plane for a 3-Dimensional dipole array at 300 MHz with mutual coupling.
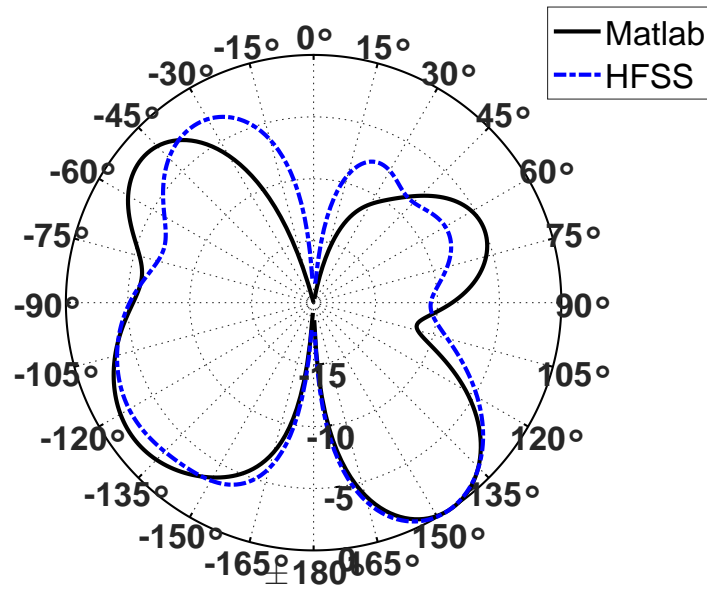
Figure 3.43: Radiation pattern comparison of HFSS and MATLAB in yz-plane for a 3-Dimensional dipole array at 300 MHz with mutual coupling.

66
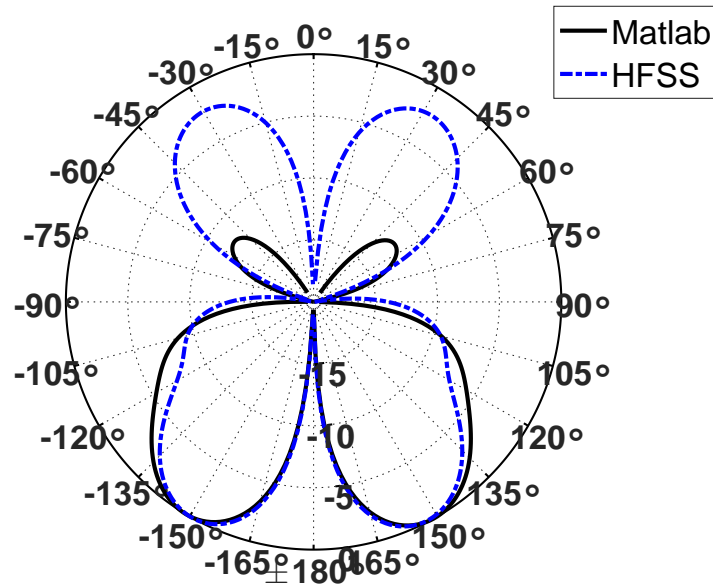
Figure 3.44: Radiation pattern comparison of HFSS and MATLAB in xz-plane for a 3-Dimensional dipole array at 300 MHz with mutual coupling.

The patterns are not exactly similar but close enough to a good approximation because in MATLAB magnetic frill current has been used as the excitation source where as in HFSS a lumped port has been used for the excitation of the antennas which results in the discrepancies.

Next, the square array case studied in Section 3.3 has been compared with HFSS. The setup is shown in Fig. 3.45.
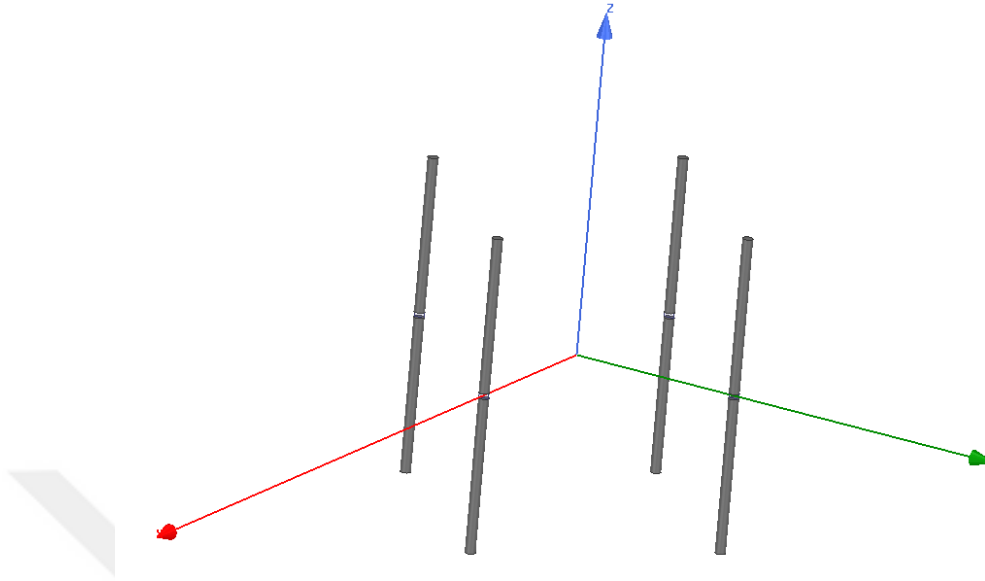
Figure 3.45: Circular array of four dipole elements in HFSS.

Figure. 3.46 shows a comparison between HFSS and MATLAB for the radiation pattern in the xy-plane when the dipoles are excited with a uniform phase progression similar to that in Section 3.3. The pattern obtained has mutual coupling effect.
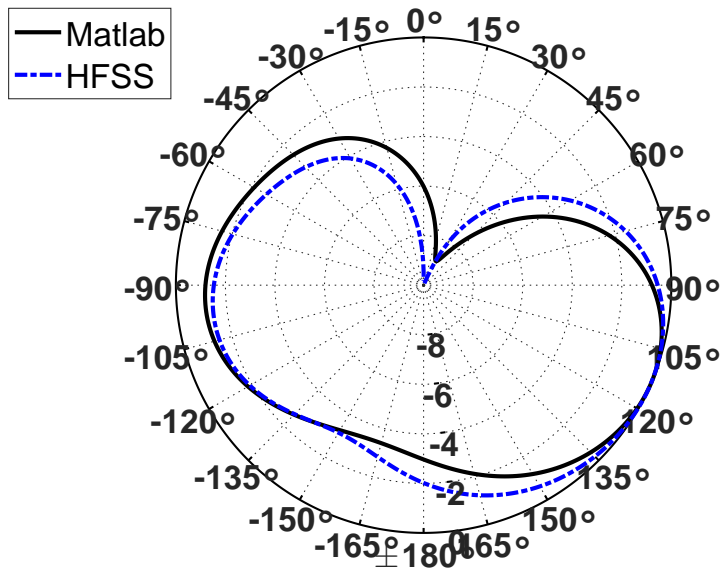
Figure 3.46: Radiation pattern comparison of HFSS and MATLAB in xy-plane for a square array excited with uniform phase progression operating at 300 MHz with mutual coupling.

Now, when the array is excited with the compensated voltages obtained from MATLAB the results are compared in Fig. 3.47.
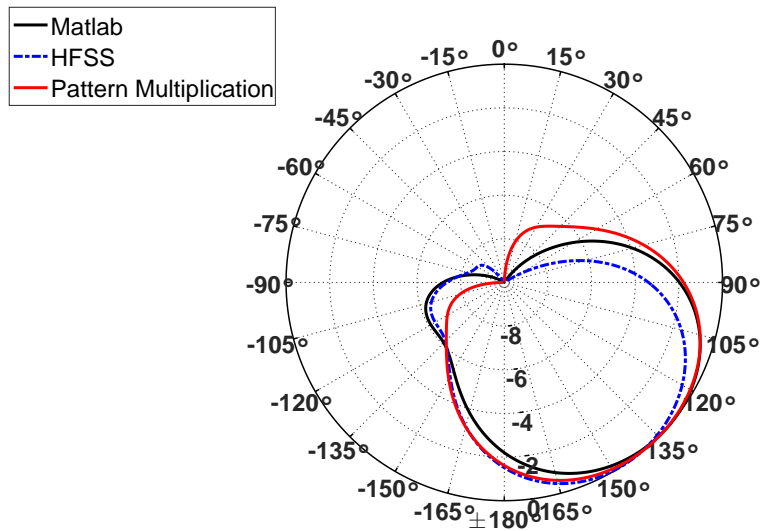
Figure 3.47: Compensated radiation patterns comparison of HFSS and MATLAB in xy-plane for a square array excited with uniform phase progression operating at 300 MHz.

Figure 3.47 shows the compensated patterns in HFSS and MATLAB in comparison with the pattern multiplication method. The contrast between Fig. 3.46 and 3.47 is evident which depicts the effect of mutual coupling and its adverse effects.

The mean square error for the polar plots in Fig. 3.33 has been calculated in the Fig. 3.48 below.
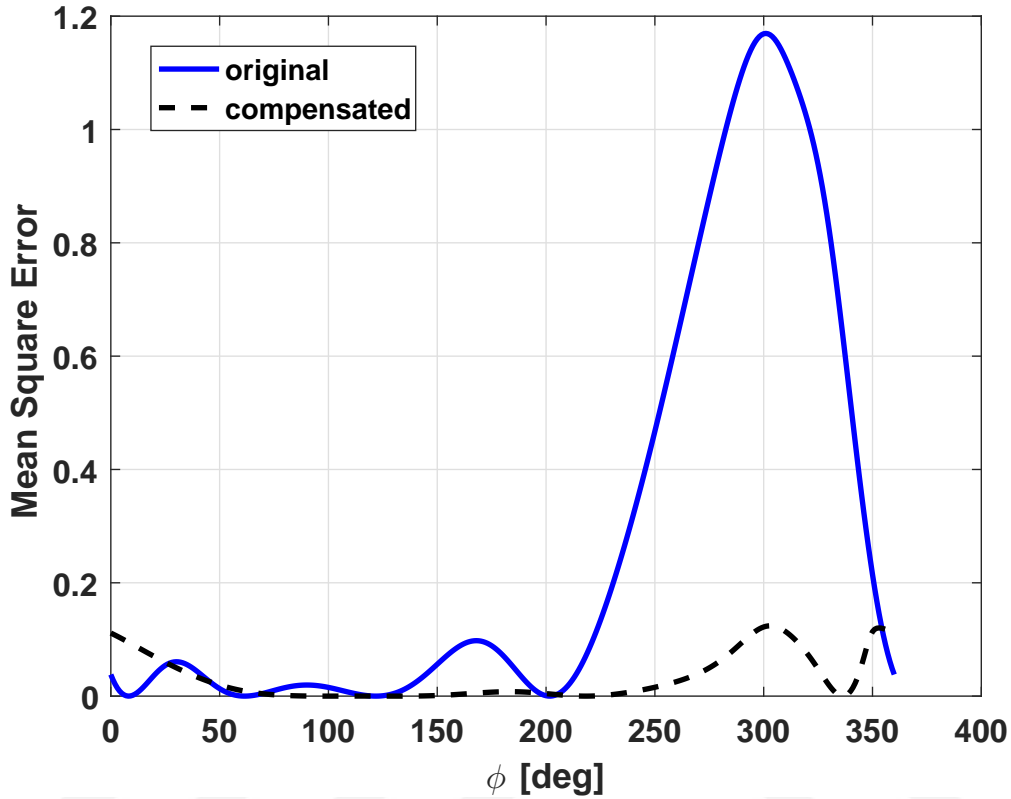
Figure 3.48: Mean Square Error for the compensation of circular array of four dipoles.

The error has been calculated for every degree in ϕ where the reference line is zero line. It can be seen that from 0° to 50° the error in the compensated pattern is less than 10% and then the error is zero till 250°. The maximum error is between 250° and 350° which is again less than 20%. These errors are in the back lobe of the radiation pattern where as in the main beam perfect compensation has been achieved. Whereas, the error in the original pattern is more than 100% between 200° to 360°.

Chapter 4

Conclusions

In this dissertation mutual coupling for thin wire antennas has been compensated. With the same antenna design mutual coupling can be compensated successfully by just modifying excitation voltages. Piecewise sinusoidal Galerkins method is the best known moment method procedure for thin wire antennas and scattering problems in free-space. Magnetic Frill modeling of the source is also an accurate model which has been used in this work. Compensation for identical, non-identical, circular, and 3-Dimensional arrays has been achieved. The results have been verified using commerical software HFSS which are in good agreement. However, there are some limitations to the method that has been implemented in this dissertation, which are listed below:

- It can be used to compensate for mutual coupling in compact antenna arrays that are less than or equal to $\lambda/2$ in length.

- Applicable to transmitting antennas, not receiving antennas but can be extended.

- Applied to thin wire antennas but can be extended.

- An approximate method, because we use thin wire antennas, and solve by numerical methods (which are approximate themselves).

- Accuracy of the solution depends on the accuracy of S parameters.

- S parameters depends on accurate computation of impedance (Moment Matrix).

Future research work will focus on using exicitations of different amplitudues in planar arrays,

e.g., binomial, triangular, uniform etc and study the effect of these different excitations on the compensation. Increasing the number of elements in the array and studying the effects of coupling and compensation. Implementing this technique for receiving antenna arrays such as massive MIMO systems. This technique can be extended to receiving antennas by studying the effect of mutual coupling as a function of direction of arrival. Accurate estimation of direction of arrival is important for massive MIMO systems. In conclusion, this study provides a fundamental understanding of the effects of mutual coupling in antenna arrays and facilitates the design of corresponding compensation techniques in practical arrays.

Bibliography

[1] W. L. Stutzman and G. A. Thiele, *Antenna theory and design*, John Wiley & Sons Inc., 3rd ed., 2013.

[2] W. L. Stutzman and G. A. Thiele, *Antenna Theory and Design*, John Wiley & Sons Inc., 1st ed., 1981.

[3] C. Balanis and C. Birtcher, "Mutual Coupling Compensation in UCAs: Simulations and Experiment," *IEEE Trans. Antennas Propag.*, vol. 54, no. 11, pp. 3082–3086, 2006.

[4] H. T. Hui, M. E. Bialkowski, and H. S. Lui, "Mutual coupling in antenna arrays," *International Journal of Antennas and Propagation*, vol. 2010, pp. 1–2, 2010.

[5] C. Craeye and D. Gonzlez-Ovejero, "A review on array mutual coupling analysis," *Radio Science*, vol. 46, no. 2, 2011.

[6] H. S. Lui, H. T. Hui, and M. S. Leong, "A note on the mutual-coupling problems in transmitting and receiving antenna arrays," *IEEE Antennas Propag. Mag.*, vol. 51, no. 5, pp. 171–176, 2009.

[7] A. C. J. Malathi and D. Thiripurasundari, "Review on isolation techniques in mimo antenna systems," *Indian Journal of Science and Technology*, vol. 9, no. 35, 2016.

[8] C. Craeye and D. Gonzlez-Ovejero, "Techniques to reduce the mutual coupling and to improve the isolation between antennas in a diversity system," 2011.

[9] H. Steyskal and J. S. Herd, "Mutual Coupling Compensation in Small Array Antennas," *IEEE Trans. Antennas Propag.*, vol. 38, no. 12, pp. 1971–1975, 1990.

[10] S. Henault and Y. M. M. Antar, "Comparison of various mutual coupling compensation methods in receiving antenna arrays," *2009 IEEE Antennas and Propagation Society International Symposium*, pp. 1–4, June 2009.

[11] R. F. Harrington, *Field Computation by Moment Methods*, Wiley-IEEE Press, 1993.

[12] L. L. Tsai, "A Numerical Solution for the Near and Far Fields of an Annular Ring of Magnetic Current," *IEEE Trans. Antennas Propag.*, vol. 20, no. 5, pp. 569–576, 1972.

[13] H. King, "Mutual impedance of unequal length antennas in echelon," *IRE Transactions on Antennas and Propagation*, vol. 5, pp. 306–313, July 1957.

[14] M. Zamlynski and P. Slobodzian, "Comment on 'compensate for the coupled radiation patterns of compact transmitting antenna arrays'," *IET Microwaves, Antennas Propagation*, vol. 8, pp. 719–723, July 2014.

[15] C. H. Niow, Y. T. Yu, and H. T. Hui, "Compensate for the coupled radiation patterns of compact transmitting antenna arrays," *IET Microwaves, Antennas Propagation*, vol. 5, pp. 699–704, April 2011.

[16] W. Gibson, *The Method of Moments in Electromagnetics*, CRC Press, 2007.

[17] E. C. Jordan and K. G. Balmain, *Electromagnetic waves and radiating systems*, Englewood Cliffs, N.J. : Prentice-Hall, 2nd ed., 1968.

Appendix A

Thin wire approximation

Consider a wire as shown in Fig. A.1 of length L and radius a illuminated by an incident plane wave. Since it is a highly conducting wire having a conductivity $\sigma \longrightarrow \infty$ we can say that the skin depth is zero since $\delta = \frac{1}{\sqrt{\pi \mu_o \sigma f}}$. Then we can deduce that all the current is flowing on the surface of the conductor and inside the fields are zero. A surface equivalent model can be seen in Fig. A.2.
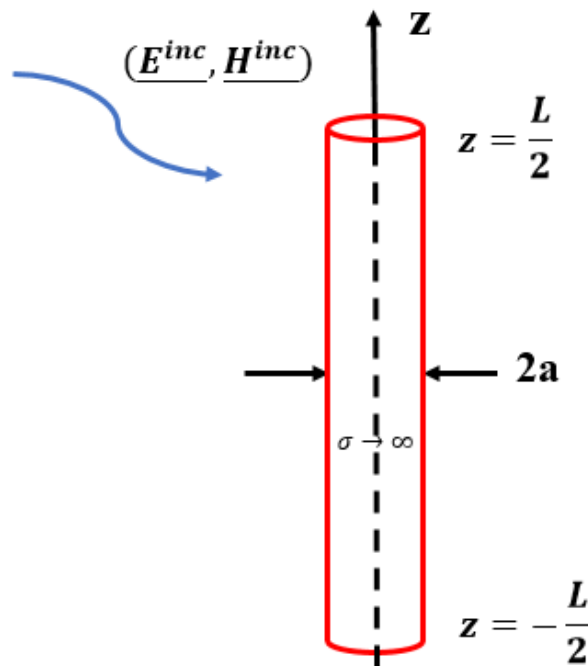
Figure A.1: A wire scatterer of length L and radius a illuminated by an incident plane wave.

The equivalent surface current $\underline{J}_s$ on (the fictitious surface) S in Fig. A.2 is actually the same as the physical current that is induced on the surface of the perfectly conducting wire in the original problem shown in Fig. A.1. Tangential component of the E-field is continuous and for PEC it is equal to zero.

$$\underline{E}_{tan} = 0 \text{ on S}$$

This $\underline{J}_s$, radiating into the unbounded medium (ϵ_o, μ_o), cancels the incident field at internal points (to S), to give the null field inside S and gives the correct fields outside S.
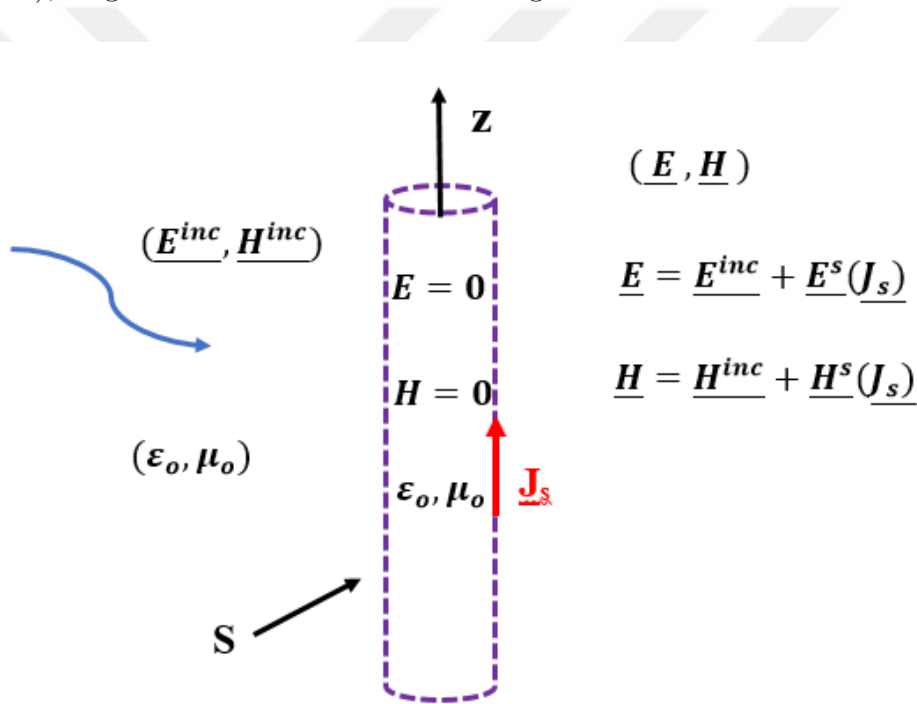
Figure A.2: Surface equivalence model with equivalent surface current density $\underline{J}_s$ in free space.

Then

$$\underline{E}_{tan}^{inc} + \underline{E}_{tan}^{s}(\underline{J}_s) = 0 \quad \text{on } S \tag{A.1}$$

$$\underline{E}_{tan}^{s}(\underline{J}_s) = -\underline{E}_{tan}^{inc} \quad \text{on } S \tag{A.2}$$

$\mathbf{J_s}$ is a surface current distribution and can vary with z and φ if it is a thick antenna. However, if the antenna is very thin i.e., $a \ll \lambda$ and $a \ll L$ then the current has no variation in φ

direction and varies only along z. When E-field has only z-component then the following equation should be solved.

$$\underline{E}_z^s(\underline{J}_z) = -\underline{E}_z^{inc} \quad \text{on } S \tag{A.3}$$

Furthermore, it is not feasible to calculate E-field produced by a current on the surface right at the surface because it is difficult to solve numerically and the integral goes to infinity. Hence, in order to remove the numerical complication due to singularity the surface current density is reduced to a line current by shrinking it to the axis of the wire. Henceforth, Eq. A.3 reduces to the following equation

$$\underline{E}_z^s(I_z') = -\underline{E}_z^{inc} \quad \text{on } S \tag{A.4}$$

The left hand side of Eq. A.4 is the z-component of the E-field produced by a current I_z', which flows on the axis of the wire, at a matched point which is on the surface of the wire at $\rho = a$. This equivalent filamentary line source can be seen in Fig. A.3.
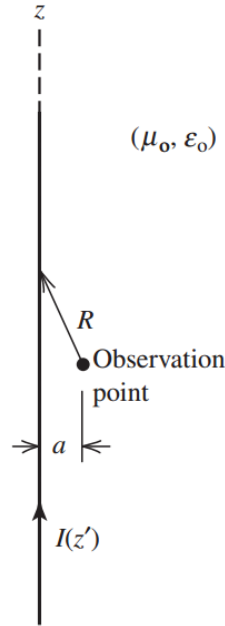

Figure A.3: Equivalent filamentary line source for a z-directed wire when wire radius $a \ll \lambda$ [1].

Equation A.4 is called **EFIE**(Electric Field Integral Equation). This is the exact equation which is solved approximately using method of moments. It can be written as,

$$\int I(z')K(z,z')dz' = -E_z^i \tag{A.5}$$

77

Here $K(z, z')$ is the Kernel of the integral equation in A.5. The integral in (A.5) is the z-component of the electric field produced by the current $I(z')$ on the axis of the antenna, at a point on the surface of the antenna. This point has cylindrical co-ordinates of $\rho = a$, $\phi = 0$ and z. The right hand side of (A.5) is the z-component of the incident field at the same point on the surface of the antenna. This field may be due to an incident plane wave or it may be produced by a voltage source at the center of the antenna. In this work we assume a voltage source as the excitation. We model this source by a magnetic frill current.

The unknown current can be written as

$$I(z') = \sum_{n=1}^{N} I_n F_n(z') \tag{A.6}$$

where $F_n(z')$ denotes the nth (known) expansion function or basis function, and I_n is the unknown expansion coefficient to be found. Possible expansion functions include entire domain sinusoidal functions, sub-domain pulses, and triangular or piecewise sinusoidal functions as shown in Fig. A.4.

(a)

(b)

(c)
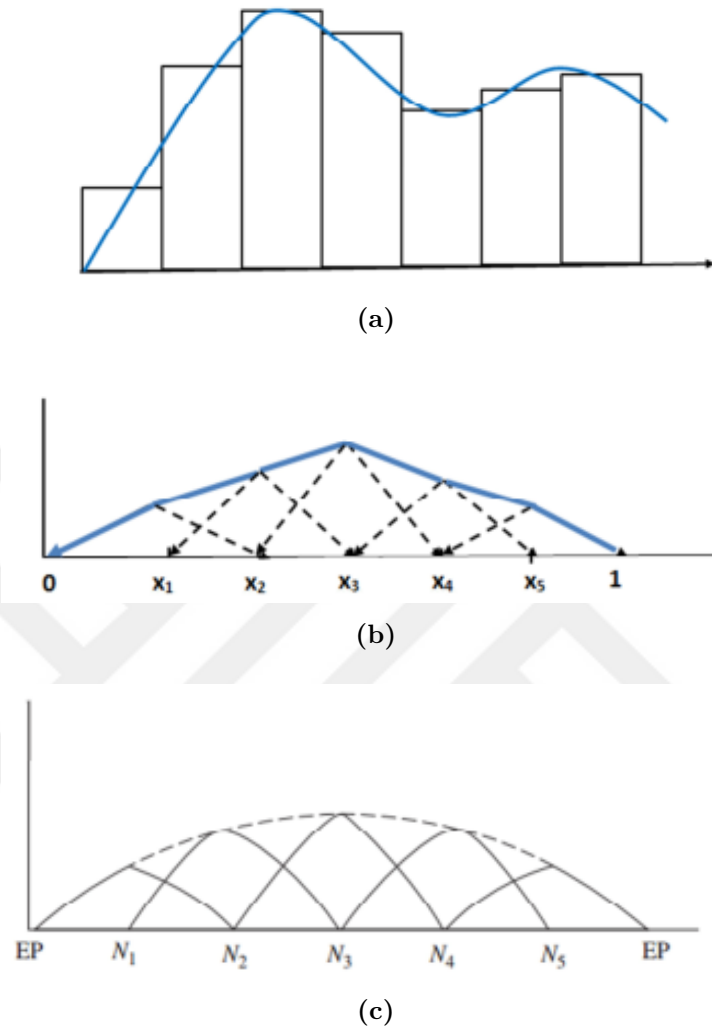
Figure A.4: Expansion functions. a) "Staircase" approximation to an actual current distribution. b) Set of overlapping triangular functions. c) Set of overlapping piecewise sinusoidal functions [1].

The basis function should reasonably approximate the unknown function over the given interval. Together the basis functions should be able to satisfy the integral equation and the boundary conditions. These are the functions which can be used to represent the current on the thin wire. Now we know that the current is zero at the ends of the wire and has an approximate sinusoidal distribution with maximum at the centre. The weighted sum of basis functions is used to represent the unknown current in MoM. One of the most useful functions in moment method solutions of thin wire problems is the piecewise sinusoid shown in Fig. A.5.
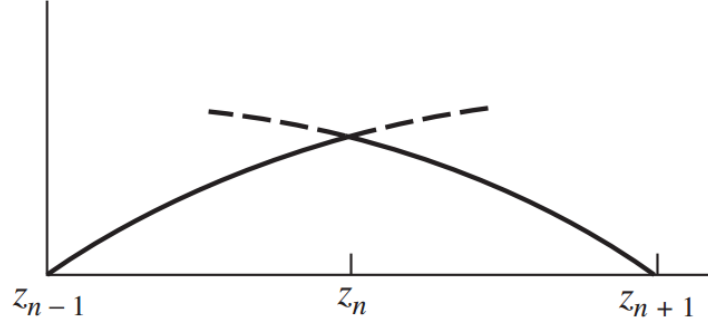
Figure A.5: Piecewise sinusoidal expansion function [1].

It may be expressed mathematically for z-directed segments by,

$$\mathbf{F_n}(z) = \hat{z}\frac{sin\beta(z - z_{n-1})}{sin\beta(z_n - z_{n-1})} \qquad z_{n-1} \leq z < z_n \qquad (A.7)$$

$$\mathbf{F_n}(z) = \hat{z}\frac{sin\beta(z_{n+1} - z)}{sin\beta(z_{n+1} - z_n)} \qquad z_n \leq z < z_{n+1} \qquad (A.8)$$

Once we decide on the expansion functions $F_n(z')$, we put Eq. A.6 into Eq. A.5 to get

$$-\int_{-L/2}^{L/2} K(z, z')\sum_{n=1}^{N} I_n F_n(z')dz' = E_z^i(z)$$

or

$$-\sum_{n=1}^{N} I_n\left[\int_{-L/2}^{L/2} K(z, z')F_n(z')dz'\right] = E_z^i(z) \qquad (A.9)$$

Note that the quantity in the square brackets is the z-component of the electric field (at a point z on the surface S) due to a known electric current distribution $F_n(z')$ along the z-axis. If $F_n(z')$ is a sub-domain basis function (that exists only in a portion $\triangle z_n'$), then the above integral will reduce to

$$\int_{\triangle z_n'} K(z, z')Fn(z')dz'$$

If we enforce Eq. A.9 at discrete points z_m (point-matching):

$$-\sum_{n=1}^{N} I_n\int_{\triangle z_n'} K(z_m, z')F_n(z')dz' = E_z^i(z_m) \qquad (A.10)$$

80

If F_n is the piecewise sinusoidal function of Fig. A.5, the integral in (A.10) is given by [17],

$$E_z = -j30I_m\left(\frac{e^{-j\beta R_1}}{R_1} + \frac{e^{-j\beta R_2}}{R_2} + 2\cos\beta H\frac{e^{-j\beta r}}{r}\right) \qquad (A.11)$$

Here I_m is a constant equal to the maximum value of F_n at its center. R_1 is the distance between the top of F_n and the field point z. R_2 is the distance from the bottom of F_n to the point z, and r is the distance from the center of F_n to z as shown in Fig. B.1. H is the half length of the domain of F_n.

Appendix B

# Formulation of the Z matrix for N-segment solution
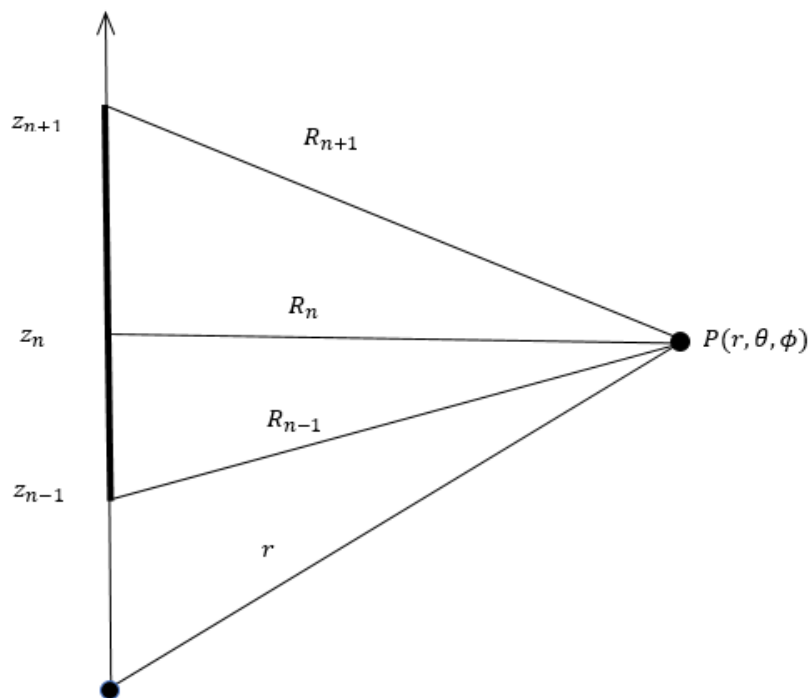
Figure B.1: Wire segment along z-axis [2].

In this work we use Galerkin's method. Then elements of the generalized impedance matrix are given in general for z-directed segments by,

$$
Z_{mn} = - \int_{z_{m-1}}^{z_{m+1}} \mathbf{I_m} \cdot \mathbf{E_n^s} dz
$$

$$
= - \left[\int_{z_{m-1}}^{z_m} \frac{\sin \beta(z - z_{m-1})}{\sin(\beta \Delta z_m)} + \int_{z_m}^{z_{m+1}} \frac{\sin \beta(z_{m+1} - z)}{\sin(\beta \Delta z_m)} \right] \frac{j30}{\sin(\beta \Delta z_n)} \qquad (\text{B.1})
$$

$$
\cdot \left[\frac{e^{-j\beta R_{n-1}}}{R_{n-1}} - 2\cos(\beta \Delta z_n) \frac{e^{-j\beta R_n}}{R_n} + \frac{e^{-j\beta R_{n+1}}}{R_{n+1}} \right] \mathbf{d}z
$$

where,

The quantities $R_{n-1}, R_n,$ and R_{n+1} are shown in Fig. B.1 and defined below.

$$
R_{n-1} = \sqrt{\rho^2 + (z - z_{n-1})^2} \,, \qquad R_n = \sqrt{\rho^2 + (z - z_n)^2}
$$
$$
R_{n+1} = \sqrt{\rho^2 + (z - z_{n+1})^2} \qquad\qquad (\text{B.2})
$$

$$
\Delta z_n = z_n - z_{n-1} = z_{n+1} - z_n, \quad \Delta z_m = z_m - z_{m-1} = z_{m+1} - z_m \qquad (\text{B.3})
$$

Equation (B.1) maybe evaluated without difficulty by numerical integration. However, when $\rho = a$ and a is quite small (i.e., wires of very small radius) it may be preferable to carry out the integration in the form of sine "Si" and cosine "Ci" integrals.

$$
Si(x) = \int_0^x \frac{sint}{t} dt \qquad\qquad (\text{B.4})
$$

$$
Ci(x) = - \int_x^\infty \frac{sint}{t} dt \qquad\qquad (\text{B.5})
$$

When this is done, the elements of Z_{mn} are given by $Z_{mn} = R_{mn} + jX_{mn}$ where,

83

$$R_{mn} = \frac{15}{\sin(\beta\Delta z_m)\sin(\beta z_n)}$$

$$[\cos\beta(z_{n-1} - z_{m-1})\{\text{Ci}(v_0) + \text{Ci}(u_0) - \text{Ci}(u_1) - \text{Ci}(v_1)\}$$

$$+ \sin\beta(z_{n-1} - z_{m-1})\{\text{Si}(v_0) - \text{Si}(u_0) + \text{Si}(u_1) - \text{Si}(v_1)\}$$

$$+ cos\beta(z_{n+1} - z_{m-1})\{\text{Ci}(v_4) + \text{Ci}(u_4) - \text{Ci}(u_5) - \text{Ci}(v_5)\}$$

$$+ \sin\beta(z_{n+1} - z_{m-1})\{\text{Si}(v_4) - \text{Si}(u_4) + \text{Si}(u_5) - \text{Si}(v_5)\}$$

$$- 2\cos(\beta\Delta z_n)\cos\beta(z_n - z_{m-1})\{\text{Ci}(v_2) + \text{Ci}(u_2) - \text{Ci}(u_3) - \text{Ci}(v_3)\}$$

$$- 2\cos(\beta\Delta z_n)\sin\beta(z_n - z_{m-1})\{\text{Si}(v_2) - \text{Si}(u_2) + \text{Si}(u_3) - \text{Si}(v_3)\} \qquad \text{(B.6)}$$

$$+ \cos\beta(z_{n-1} - z_{m+1})\{\text{Ci}(v_6) - \text{Ci}(v_1) + \text{Ci}(u_6) - \text{Ci}(u_1)\}$$

$$+ \sin\beta(z_{n-1} - z_{m+1})\{\text{Si}(v_6) - \text{Si}(u_6) + \text{Si}(u_1) - \text{Si}(v_1)\}$$

$$+ \cos\beta(z_{n+1} - z_{m+1})\{\text{Ci}(v_8) - \text{Ci}(v_5) - \text{Ci}(u_5) + \text{Ci}(u_8)\}$$

$$+ \sin\beta(z_{n+1} - z_{m+1})\{\text{Si}(v_8) - \text{Si}(u_8) + \text{Si}(u_5) - \text{Si}(v_5)\}$$

$$- 2\cos(\beta\Delta z_n)\cos\beta(z_n - z_{m+1})\{\text{Ci}(v_7) - \text{Ci}(v_3) - \text{Ci}(u_3) + \text{Ci}(u_7)\}$$

$$- 2\cos(\beta\Delta z_m)\sin\beta(z_n - z_{m+1})\{-\text{Si}(u_7) + \text{Si}(v_7) + \text{Si}(u_3) - \text{Si}(v_3)\}]$$

$$u_0 = \beta[\sqrt{\rho^2 + (z_{n-1} - z_{m-1})^2} + (L)(z_{m-1} - z_{n-1})] \qquad \text{(B.7a)}$$

$$u_1 = \beta[\sqrt{\rho^2 + (z_{n-1} - z_m)^2} + (L)(z_m - z_{n-1})] \qquad \text{(B.7b)}$$

$$u_2 = \beta[\sqrt{\rho^2 + (z_n - z_{m-1})^2} + (L)(z_{m-1} - z_n)] \qquad \text{(B.7c)}$$

$$u_3 = \beta[\sqrt{\rho^2 + (z_n - z_m)^2} + (L)(z_m - z_n)] \qquad \text{(B.7d)}$$

$$u_4 = \beta[\sqrt{\rho^2 + (z_{n+1} - z_{m-1})^2} + (L)(z_{m-1} - z_{n+1})] \qquad \text{(B.7e)}$$

$$u_5 = \beta[\sqrt{\rho^2 + (z_{n+1} - z_m)^2} + (L)(z_m - z_{n+1})] \qquad \text{(B.7f)}$$

$$u_6 = \beta[\sqrt{\rho^2 + (z_{n-1} - z_{m+1})^2} + (L)(z_{m+1} - z_{n-1})] \qquad \text{(B.7g)}$$

$$u_7 = \beta[\sqrt{\rho^2 + (z_n - z_{m+1})^2} + (L)(z_{m+1} - z_n)] \qquad \text{(B.7h)}$$

$$u_8 = \beta[\sqrt{\rho^2 + (z_{n+1} - z_{m+1})^2} + (L)(z_{m+1} - z_{n+1})] \qquad \text{(B.7i)}$$

and $L = +1$. The v_i's are found in similar manner as (B.7) with $L = -1$. X_{mn} can be obtained by replacing Ci(x) by -Si(x) and Si(y) by Ci(y) in the expression for R_{mn}. The piecewise sinusoidal Galerkin method is the best known moment procedure for thin wire antenna and scattering problems in free space. The piecewise sinusoidal Galerkin method applies equally well to arbitrary configurations of wires [2].

Appendix C

Source Modeling

Consider Fig. C.1a which shows a coaxial line feeding a monopole on a ground plane. We can replace the ground plane and the coaxial aperture with a frill of magnetic current assuming a purely dominant mode distribution (TEM) in the coaxial aperture, as shown in Fig. C.1b Since the assumed form of the electric field in the aperture is,

$$E_{\rho'}(\rho') = \frac{1}{2\rho'\ln(b/a)} \tag{C.1}$$

the corresponding magnetic current distribution is,

$$M_{\phi'} = \frac{-1}{\rho'\ln(b/a)} \tag{C.2}$$

from which it can be shown that the electric field on the axis of the monopole is,

$$E_z^i(0, z) = \frac{1}{2\ln(b/a)} \left(\frac{e^{-j\beta R_1}}{R_1} - \frac{e^{-j\beta R_2}}{R_2} \right) \tag{C.3}$$

where,
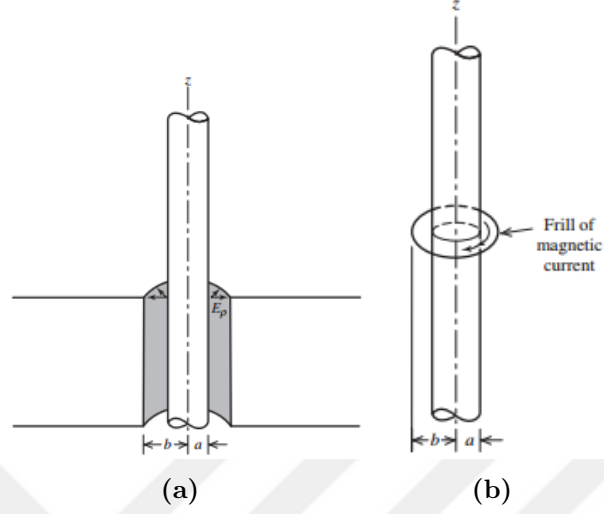
Figure C.1: a) Coaxial line feeding a monopole through a ground plane. b) Mathematical model of (a) [1].

$$R_1 = \sqrt{z^2 + a^2} \tag{C.4a}$$

$$R_2 = \sqrt{z^2 + b^2} \tag{C.4b}$$

if the frill center is at the coordinate origin [1]. Elements of the generalized voltage matrix are given in general by ,

$$V_m = -\int_{z_{m-1}}^{z_{m+1}} \mathbf{I_m} \cdot \mathbf{E_z^i} dz$$

$$V_m = -\left[\int_{z_{m-1}}^{z_m} \frac{\sin\beta(z - z_{m-1})}{\sin(\beta\Delta z_m)} + \int_{z_m}^{z_{m+1}} \frac{\sin\beta(z_{m+1} - z)}{\sin(\beta\Delta z_m)}\right] \tag{C.5}$$

$$\cdot \frac{1}{2\ln(b/a)}\left[\frac{e^{-j\beta R_1}}{R_1} - \frac{e^{-j\beta R_2}}{R_2}\right] dz$$

COMPENSATION OF MUTUAL COUPLING IN TRANSMITTING ARRAYS OF THIN WIRE ANTENNAS